Effects of idealised land cover and land management changes on the atmospheric water cycle

Steven J. De Hertog[1], Carmen E. Lopez-Fabara[1], Ruud van der Ent[2], Jessica Keune[3], Diego G. Miralles[3], Raphael Portmann[4], Sebastian Schemm[5], Felix Havermann[6], Suqi Guo[6], Fei Luo[7,8,9], Iris Manola[7], Quentin Lejeune[10], Julia Pongratz[6,11], Carl-Friedrich Schleussner[10], Sonia I. Seneviratne[5], and Wim Thiery[1]

[1]Vrije Universiteit Brussel, Department of Water and Climate, Brussels, Belgium
[2]Delft University of Technology, Department of water management, Delft, Netherlands
[3]Ghent University, Hydro-Climate Extremes Lab, Ghent, Belgium
[4]Agroscope Reckenholz, Division of Agroecology and Environment, Zurich, Switzerland
[5]ETH Zurich, Institute for Atmospheric and Climate Science, Zurich, Switzerland.
[6]Ludwig-Maximilians-University Munich, Department of Geography, Munich, Germany
[7]Vrije Universiteit Amsterdam, Institute for Environmental studies, Amsterdam, Netherlands
[8]Royal Netherlands Meteorological Institute (KNMI), De Bilt, Netherlands.
[9]Centre for Climate Research Singapore (CCRS), Singapore.
[10]Climate Analytics, Berlin, Germany
[11]Max Planck Institute for Meteorology, Hamburg, Germany

Correspondence: Steven De Hertog (steven.de.hertog@vub.be)

Abstract. Land cover and land management changes (LCLMCs) play an important role in achieving low-end warming scenarios through land-based mitigation. However, their effects on moisture fluxes and recycling remain uncertain although they have important implications for the future viability of such strategies. Here, we analyse the impact of idealised LCLMC scenarios on atmospheric moisture transport in three different ESMs: the Community Earth System Model (CESM), the Max Planck Institute Earth System Model (MPI-ESM) and the European Consortium Earth System Model (EC-EARTH). The LCLMC

5   scenarios comprise of a full cropland world, a fully afforested world, and a cropland world with unlimited irrigation expansion. The effects of these LCLMCs in the different ESMs are analysed for precipitation, evaporation and vertically integrated moisture flux convergence to understand the LCLMC-induced changes in the atmospheric moisture cycle. Then, a moisture tracking algorithm is applied to assess the effects of LCLMCs on moisture recycling at the local (grid cell level) and the global scale (continental moisture recycling). Our results indicate that LCLMCs are generally inducing consistent effects on moisture fluxes

10   over land in all ESMs. Cropland expansion causes drying and reduced local moisture recycling in all ESMs, while afforestation and irrigation expansion generally cause wetting and increased local moisture recycling. However, the strength of this influence varies in time and space and across the ESMs and shows a strong dependency on the dominant driver: Some ESMs show a dominance of large scale atmospheric circulation changes while other ESMs show a dominance of local to regional changes in the atmospheric water cycle only within the vicinity of the LCLMC. Overall, these results corroborate that LCLMCs can induce

15   large effects on the atmospheric water cycle and moisture recycling, but more research is needed to constrain the uncertainty of these effects within ESMs and better evaluate land-based mitigation strategies.

Earth System
Dynamics
Discussions

1 Introduction

Currently, about three quarters ($\sim$100 $*10^6$ km^2) of the ice-free land surface has undergone some kind of anthropogenic land
cover or land management change (LCLMC) (Luyssaert et al., 2014; Mbow et al., 2017). All these modifications are important
drivers of climate change as they alter the carbon cycle (biogeochemical effects) and affect surface properties, which impact
the energy and water balance (biogeophysical effects) (Pongratz et al., 2010; Bonan, 2008; Pongratz et al., 2021) and feed
back on the local to global climate (Winckler et al., 2019; Boysen et al., 2020; Portmann et al., 2022; De Hertog et al., 2023).
Therefore, future LCLMCs are increasingly seen as a viable tool for land based mitigation and play a crucial role within low
warming emission scenarios (Rogelj et al., 2018; Seneviratne et al., 2018). Hence, exploring and understanding the extent to
which LCLMCs influence climate has become key to develop effective mitigation and adaptation strategies (Lawrence et al.,
2016).

From a biogeophysical perspective, LCLMCs lead to changes in the albedo, aerodynamic conductance and the partition-
ing between the sensible and latent heat flux which has an impact on atmospheric temperature and moisture content (Bowen,
1926; Wang et al., 2009). For example, tropical deforestation is expected to further dry and warm the regional climate (Bonan,
2008; Akkermans et al., 2014; Spracklen et al., 2018). In contrast, irrigation expansion can cause a local to regional cooling
and moistening of the atmosphere (Mahmood et al., 2014; Thiery et al., 2017, 2020; Hauser et al., 2019; Tuinenburg et al.,
2014). Evaporation, being the link between the surface energy and the water balance (Shukla and Mintz, 1982), modulates
the influence of LCLMCs on atmospheric conditions (van der Ent et al., 2010; Spracklen et al., 2012). Tracking the origins
of precipitation back to evaporation and determining the fraction of terrestrial precipitation that originates from land — here
referred to as continental precipitation recycling (van der Ent et al., 2010) — can increase our understanding of the effects of
future LCLMCs on the climate. On the other hand, the fate of land evaporation can be determined and illustrates the reach of
local LCLMCs; the fraction of terrestrial evaporation precipitating over land is often referred to as continental evaporation re-
cycling (van der Ent et al., 2010). Even though, it is well established that LCLMC can affect these moisture recycling strengths
(Wang-Erlandsson et al., 2018; Benedict et al., 2020) — i.e., the degree to which terrestrial precipitation depends on land
evaporation — this is rarely quantified within dedicated ESM studies. Most studies that quantify the effects of LCLMCs on the
atmospheric moisture cycle focus on the changes in moisture fluxes, but often cannot unravel the role of local and continental
moisture recycling in these differences (Tuinenburg et al., 2020; Hoek van Dijke et al., 2022; Baudena et al., 2021; Wunder-
ling et al., 2022; Staal et al., 2018). Those studies that do account for moisture recycling in assessing the effects of LCLMC
generally apply reanalysis based recycling ratios (Tuinenburg et al., 2020; Hoek van Dijke et al., 2022; Baudena et al., 2021;
Wunderling et al., 2022; Staal et al., 2018) which do not include the two-way interactions of circulation changes and the water
cycle. By analysing dedicated ESM simulations for LCLMC we are able to address these shortcomings and include the effects
of atmospheric circulation changes on moisture recycling.

Idealized or extensive implementations of LCLMCs within ESM simulations are used to cope with weather-induced noise that dampens climatic responses (Winckler et al., 2017a; Boysen et al., 2020). Within such simulations, large-scale atmospheric circulation changes have been shown to occur as a consequence of LCLMC (Goessling and Reick, 2011; Boysen et al., 2020; Portmann et al., 2022; Devaraju et al., 2018; Laguë et al., 2019). However, most studies have only focused on one LCLMC type

55 (e.g. Boysen et al., 2020; Laguë et al., 2019; Devaraju et al., 2018)) and only used a single ESM (e.g. Portmann et al., 2022; de Vrese et al., 2016). Further, these studies generally cannot distinguish explicitly between the influence of local processes (directly induced by the LCLMC) and non-local or remote processes (induced by LCLMC elsewhere, including circulation and advection changes). The study of De Hertog et al. (2023) presented a first multi-model intercomparison using three different ESMs and four different LCLMC types in which a clear distinction between local and non-local biogeophysical effects was

60 established through the checkerboard LCLMC implementation as developed by Winckler et al. (2017a). These simulations facilitated the comparison of the climate changes induced by different LCLMC types and to grasp the multi-model uncertainty.

Here, we assess the atmospheric water cycle responses to idealised LCLMC scenarios using global simulations of three different ESMs (De Hertog et al., 2023). The simulations comprise different idealised LCLMC scenarios — from afforestation,

65 over cropland expansion to irrigation expansion — and have been implemented in a checkerboard pattern. The simulation setup and the moisture tracking algorithm and its derived metrics are described below (Section 2). We first analyse the ESM output for changes in the atmospheric water cycle including evaporation, precipitation, and atmospheric moisture flux convergence (Section 3.1). Second, we analyse the moisture tracking algorithm output to assess the direct effects of LCLMCs on moisture recycling and unravel local and remote drivers of the analysed moisture flux changes. This is done on a local scale using the

70 concept of 'length scales' of moisture recycling (Section 3.2), and on a continental scale using continental recycling ratios (Section 3.3). Finally we highlight the most important findings and implications of this research (Section 4. and 5.).

2 Methods

2.1 ESM simulations

75 The ESM simulations analysed here were conducted within the LAnd MAnagement for CLImate Mitigation and Adaptation (LAMACLIMA) project and are presented in detail in De Hertog et al. (2023). In this project, different sensitivity experiments were performed for three ESMs, i.e., the Community Earth System Model version 2.1.3 (CESM), the European Community Earth-System Model 3-Veg v3.3.3.1 (EC-EARTH), and the Max-Planck Institute Earth System Model 1.2 low resolution (MPI-ESM). We refer to De Hertog et al. (2023) for detailed model descriptions. The experiments comprise four simulations

80 of LCLMC scenarios. One scenario is the control case (hereafter referred to as CTL), which is conducted with a constant land cover corresponding to the year 2015. The three remaining scenarios represent an extreme case of single specific LCLMC, namely afforestation (FRST), cropland expansion (CROP), and irrigation expansion (IRR). Here, irrigation is applied on top of the cropland expansion. Thus, while the impact of afforestation and cropland expansion is always evaluated with respect to the

control simulation (i.e., differences are calculated as FRST–CTL and CROP-CTL), the impact of irrigation is evaluated with
85   respect to the cropland expansion simulation (IRR-CROP). All simulations cover a period of 160 years under a present-day
climate forcing (corresponding to the year 2015).

The LCLMC scenarios are generated from the CTL scenario land cover by inducing the LCLMC in a checkerboard-like
pattern as presented in Winckler et al. (2017a). The resulting LCLMC is shown in Figure 1. This implies that the different
90   LCLMCs are implemented in every other pixel (i.e. only 50% of hospitable land grid cells have undergone LCLMC), while
all other forcings (i.e. greenhouse gas, stratospheric aerosols,...) remain identical to the initial CTL scenario configurations.
Even though, a structured approach was taken to implement the LCLMCs in the different ESMs, the geographical extent of
irrigation and afforestation differs strongly among different ESMs due to each model's native schemes on irrigation and the
transition to forest. This is especially the case for the EC-EARTH afforestation simulation, in which the afforestation simulated
95   was extremely low compared to the other ESMs (Figure 1d,e,f). Therefore, the afforestation scenario from EC-EARTH is not
considered in this study. Likewise, large discrepancies regarding the simulated irrigation expansion are related to different
irrigation parameterisations being implemented in the different ESMs (see appendix B in De Hertog et al., 2023). Within the
model version of EC-EARTH used in this study, irrigation does not cause any effect on atmospheric moisture content (i.e. the
water cycle of the land and atmosphere model are not coupled). Hence, the irrigation expansion scenario from EC-EARTH is
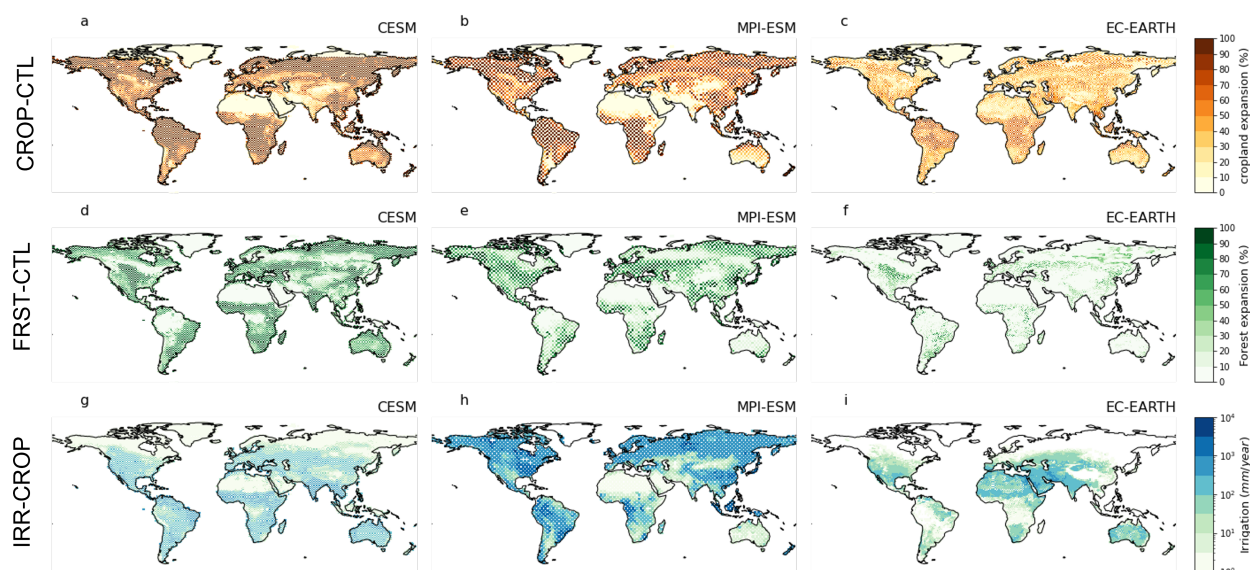100   also not considered in this study.

Figure 1. Land cover and land management changes as implemented in the three different ESMs. Cropland expansion (CROP-CTL ; a, b, c), afforestation (FRST-CTL ; d, e, f), and irrigation expansion (IRR-CROP ; g, h, i) implemented in CESM, MPI-ESM, and EC-EARTH, respectively. Both, cropland expansion and afforestation, are shown as a change in area fraction (%) while irrigation expansion is shown through the irrigation flux in mm/year.

This implementation of the LCLMCs in the ESM land cover maps following a checkerboard pattern enables a signal separation of the ESM response into local and non-local components (Winckler et al., 2017a; De Hertog et al., 2023). The local effects refer to climate effects directly induced by the LCLMC within the grid cell, while the non-local effects refer to climate effects induced by LCLMC elsewhere through changes in atmospheric circulation or advection. These non-local effects can

105 be directly derived from the simulation output as the climate changes occurring over grid cells where no land cover change occurred can only be caused by non-local mechanisms. By interpolating the values of non-local effects within the 'no change' grid cells to the 'change' grid cells we create a global map of non-local effects due to a certain LCLMC. This global map is then used to subtract the values found in the 'change' grid cells, which contain the total signal (i.e. local and non-local effects). After subtraction we obtain values for the local effects over all 'change' grid cells. These are again interpolated to create a

110 global map representing the local climate effects. This approach has been explained in detail in previous studies (Winckler et al., 2017a; De Hertog et al., 2023) and is also explained in more detail here in Appendix A.

This separation is only applicable to (near-)surface variables and not to variables representing processes that extend higher into the atmosphere, as there is lateral mixing between different adjacent atmospheric grid cells above the surface. Therefore,

115 the signal separation approach is not applied to the atmospheric variables (i.e. variables that have a vertical dimension into the atmosphere). As the analysis presented here focuses on atmospheric processes, specifically moisture recycling, which is computed through a moisture tracking algorithm requiring atmospheric variables, we are not able to separate local and non-local effects for all results in this study. Instead, we analyse the raw ESM output directly, which represents an extreme case of LCLMC applied in a checkerboard pattern. For the variables where signal separation can be applied, we provide those results

120 to support interpretations of these signals. All calculations are applied over the last 30 years of the simulations and at each ESM's native spatial resolution (latitude x longitude) (i.e., MPI-ESM: 1.88° x 1.88°, CESM: 0.90° x 1.25°, EC-EARTH: 0.7°x 0.7°).

2.2 LCLMC-induced impact on the net water fluxes

125 To understand the net change in the atmospheric water cycle induced by the different LCLMCs, we first analyse their effects on evaporation and precipitation and compare them to the reference simulation of each LCLMC scenario. In addition, the vertically integrated moisture flux convergence (MFC) is computed using the basic principles of conservation of water vapor (Banacos and Schultz, 2005; Cook, 2009; Thiery et al., 2016; Van de Walle et al., 2020), as shown in Eq. 1 below.

$$P - E \approx -\frac{1}{g\rho_w} \int\limits_{p_s}^{p\text{TOA}} (\boldsymbol{\nabla} \cdot q\boldsymbol{v})\,dp \qquad (1)$$

130 Where g is the gravitational acceleration [m/s^2], ρ_w is the density of water (1000 kg/m^3), ps and $pTOA$ is the pressure at surface level and top of the atmosphere respectively, q represents the specific humidity of an air parcel [kg/kg], $\boldsymbol{v}$ its horizontal

wind vector [m/s], P is the precipitation flux per unit area [m/s], E is the surface evaporation flux per unit area [m/s]. $\nabla \cdot (q\boldsymbol{v})$ is the atmospheric moisture convergence from the surface to the top of the atmosphere (TOA). The MFC is computed based on 6-hourly data along the available pressure levels of each ESM. For EC-EARTH, only eight atmospheric levels were available,

135 which is insufficient to compute MFC. Hence, $P - E$ is used as a proxy for the MFC in EC-EARTH. Over land, MFC or $P - E$ are often used a proxy for water availability (Van de Walle et al., 2020; Thiery et al., 2016), and changes of these measures can help understand the impacts of LCLMCs on the redistribution of water over land. The maps for MFC and $P - E$ changes are included in Appendix D.

140 The comparison of P, E, and MFC changes with respect to the corresponding reference simulation is performed for the three different LCLMC scenarios, i.e., cropland expansion, afforestation, and irrigation. We focus on annual mean values for the analysis. However, seasonal means (DJF: December, January, February; JJA: June, July, August) are shown in Appendix C. As explained in Sect. 2.1 we only apply the signal separation to P and E and not MFC as this metric is computed based on variables covering the entire atmospheric column.

145 ## 2.3 Moisture tracking analysis

To further quantify the direct influence of LCLMCs on precipitation and unravel the reach of locally-induced LCLMC on precipitation and water availability, we perform a moisture tracking analysis. Here, we apply the Eulerian moisture tracking model WAM-2layers (van der Ent et al., 2014; Benedict et al., 2020) to identify the origin of precipitation and the fate of evaporation in the ESM simulations and to evaluate the impact of LCLMC-induced evaporation changes on precipitation

150 and water availability. The output of WAM-2layers is then used to compute several metrics relevant to moisture recycling, which can help uncover LCLMC-induced effects within the different ESMs. In this study, we focus on two spatial scales of moisture recycling: (i) local recycling and (ii) continental recycling. Note that local recycling does not imply that only the local effects (following the signal separation approach explained above) are used for the computation of this metric. The moisture tracking algorithm is applied on the raw ESM data as it requires atmospheric variables which cannot be signal separated. Local

155 moisture recycling is defined on the grid-cell area of each ESM, which differs by definition (see Sect. 2.1) and makes them hard to compare across the ESMs. Therefore, additional area-independent metrics are used. Evaporation and precipitation length scales (van der Ent et al., 2010) illustrate the distance that moisture travels on average to or from a given grid cell. In the following, all recycling metrics are presented at annual time scales. Details on the setup of WAM-2layers and the definition of moisture recycling metrics are presented in more detail in the following sections.

160 ### 2.3.1 WAM-2layers

A moisture tracking algorithm, the Water Accounting Model - 2 layers (WAM-2layers, van der Ent et al. (2014)), is applied to analyse the effects of the different LCLMCs on moisture recycling. We use a recent version of this algorithm, which was modified to ingest climate model data with limited vertical levels (Benedict et al., 2020). This moisture tracking algorithm uses a Eulerian approach to solve the atmospheric moisture balance over each grid cell and a specified time step (van der Ent et al.,

Earth System
Dynamics
Discussions

Open Access

165 2014). Model outputs comprise the origins of precipitation or evaporation at the local scale or continental scale depending on
which tracking is performed, and facilitate the quantification of local and continental moisture recycling measures (van der
Ent et al., 2010; van der Ent et al., 2014, see below). The algorithm has been applied numerous times in recent years for ESM
output (Benedict et al., 2020; Guo et al., 2020; Findell et al., 2019; Bosmans et al., 2020).

Here, the surface and atmospheric data from all ESM simulations at the original spatial resolution (see Sect. 2.1) and the
170 finest temporal resolution (CESM: 6 hours, MPI-ESM: 3 hours for surface variables and 6hr for atmospheric variables, EC-
EARTH: 6 hours for surface variables and daily for atmospheric variables) are used as (offline) inputs for WAM-2layers. To
avoid stability problems related to the numerical discretisation in WAM-2layers (van der Ent et al., 2014), all ESM forcings are
linearly interpolated to 15-min time steps. The moisture tracking is applied to the last 30 years within the 160-year simulation
period.

175

2.3.2 Local moisture recycling

Here, two definitions of local moisture recycling are used. First, the local precipitation recycling ratio ρ_r, i.e. the fraction of
precipitation over a region r that originates from evaporation over the same region (see Eq. 2), is calculated. The remaining
fraction of precipitation over that region (i.e., $1-\rho_r$) originates from evaporation upwind that is advected into the region r, and
180 can be of either land or oceanic origin. Second, the local evaporation recycling ratio ϵ_r, i.e. the fraction of evaporation from a
region r that falls as precipitation over the same region (see Eq. 3), is used. The remaining fraction of local evaporation $(1-\epsilon_r)$
is transported away from the region and falls downwind of that region as precipitation.

Using the output from WAM-2layers, precipitation over the region r with area A_r, here referred to as P, can be separated
into the precipitation originating from the same region (P_r) and the remaining precipitation that originates from upwind regions
185 (P_a), so that $P = P_r + P_a$. Using these outputs, the local precipitation recycling ratio can be calculated as

$$\rho_r = \frac{P_r}{P}.\tag{2}$$

Similarly, the local evaporation recycling ratio can be calculated using evaporation from the region r, here referred to as E,
and the evaporation that falls as precipitation over the same region (E_r), i.e.

$$\epsilon_r = \frac{E_r}{E}.\tag{3}$$

190 Both local recycling definitions are subject to the area of the region considered (A_r). Here, local recycling is defined on the
area of a grid cell. It is noted that this area varies with latitude per definition and, in addition, varies for the ESM simulations
employed here (see Sect. 2.1). The differences between local recycling ratios thus need to be interpreted with caution and
are not comparable across different data sources or ESMs. To overcome these shortcomings we compute length ratios and
continental recycling ratios.

2.3.3 Precipitation and evaporation length scales

To assess local moisture recycling independently of the ESM, we compute the length scale of the moisture recycling process as introduced by van der Ent and Savenije (2011). Here we summarise the derivation of extracting the length scale metric from local moisture recycling ratios, for the complete derivation of how length scales are defined we refer to van der Ent and Savenije (2011). Following (Dominguez et al., 2006), the moisture recycling ratio is a function of the distance travelled along a streamline (x), the horizontal wind speed (u) and the moisture flux (M) normalized by the atmospheric storage capacity (S_a):

$$\gamma_r(x) = 1 - [\exp(-\frac{M}{S_a u} x)] \tag{4}$$

Here, $\gamma_r(x)$ is the moisture recycling ratio (which can be evaporation or precipitation recycling as defined in Eqs.(2) and (3)), and M is evaporation (E) for the evaporation recycling ratio and precipitation (P) for the precipitation recycling ratio. This equation is valid for a streamline starting at distance x=0. By definition, the recycling ratio equals one at the origin (x=0) and also in case of zero moisture uptake (M=0). With increasing moisture uptake and distance to the source region, the ratio tends exponentially towards zero, which indicates that the original moisture taken up at the source location is removed from the air. van der Ent and Savenije (2011) subsequently rewrote this equation of the local moisture recycling ratio as a function of the length scale (λ_γ):

$$\lambda_\gamma = \frac{S_a u}{M} \tag{5}$$

By then filling in Eq. 5 in Eq. 4 and integrating it for the distance x an equation is obtained for the regional average moisture recycling γ_r:

$$\gamma_r = \frac{\Delta x + \lambda_\gamma \exp(\frac{\Delta x}{\lambda_\gamma}) - \lambda_\gamma}{\Delta x} \tag{6}$$

Here, γ_r is the moisture recycling ratio over a given region r, with r representing a single grid cell in order to compute the length scale at the local, grid cell level. Δx equals the representative length of a grid cell and is computed from the zonal and meridional lengths of a grid cell weighted by the moisture fluxes in the corresponding directions (van der Ent and Savenije, 2011). From this equation the length scale can be isolated and solved based on the local moisture recycling to get the following expression using W as the Lambert W-Function (e.g. Corless et al., 1996).:

$$\lambda_\gamma = \frac{\Delta x}{W[\frac{\exp(\frac{1}{\gamma_r - 1})}{\gamma_r - 1}] + \frac{1}{1 - \gamma_r}} \tag{7}$$

Length scales overcome one of the major shortcomings of local recycling ratios, which are dependent on the shape and size of the source region they are computed over (van der Ent and Savenije, 2011; Theeuwen et al., 2023), which is normally problematic with regular latitude-longitude grids in which grid cells vary both in shape and size within a model as well as between

models that applied different resolutions. Length scales of local moisture recycling, in contrast, are designed to be area- and shape-independent at least for the region over which one can assume the same climatological conditions (i.e., the variables in Eq. 7 do not change much across nearby grid cells). The length scales give an indication of the distance over which moisture
225 would travel on average to or from a given grid cell under the given local hydrological and climatological conditions (van der Ent and Savenije, 2011). Hence, they should not be interpreted as actual travel distance, but rather as a local process-based metric of moisture recycling strength (Eq. 5)) expressed in distance units (km). A short length scale indicates that local recycling is strong and a long length scale indicates that local recycling is weak.

230   Like local recycling ratios, the length scales can be calculated from a precipitation- or an evaporation-centric perspective (i.e., precipitation recycling ratios λ_ρ or evaporation recycling ratios λ_ϵ). Here the precipitation length scale represents the length scale of precipitation raining down in a given grid cell, and the evaporation length scale represents the length scale of evaporation that travels from a given grid cell before precipitating. Both length scales can be derived from the local recycling ratios presented above (see section 2.3.2). By computing these different length scales for the different simulations representing
235 the different LCLMC, we can assess how the LCLMC affects precipitation and evaporation recycling strength.

2.3.4   Continental moisture recycling

To study the continental contribution to moisture recycling, we compute the continental recycling ratios. Analogous to previous studies (e.g. Brubaker et al., 1993; van der Ent et al., 2010; Gimeno et al., 2012; Findell et al., 2019; Gimeno et al., 2020), we
240 define continental precipitation recycling ratio ρ_c as the fraction of precipitation over land that originates from land evaporation. The precipitation recycling ratio answers the question 'how much of the moisture precipitating over land originates from land?'. The remaining fraction $(1 - \rho_c)$ of the precipitation over land originates from evaporation over oceans. Similarly, continental evaporation recycling ratio ϵ_c is defined as the fraction of land evaporation that falls as precipitation over land. These ratios can be computed through equations (2) and (3) by defining the region r as all land areas. Hence, in contrast to the local recycling
245 ratios, continental recycling ratios refer to the same area, i.e. the area of all continental land regions A_c, which facilitates a direct comparison of recycling ratios between the ESMs with different spatial resolution employed here. Continental evaporation and precipitation are computed by tracking all continental moisture fluxes at the same time.

3   Results

3.1   Changes in atmospheric moisture fluxes due to LCLMC

250 All ESMs generally show a decrease in evaporation over land due to cropland expansion and an increase in evaporation due to afforestation and irrigation expansion (Figure 2). However, some of the ESMs' regional signals deviate from this general pattern. For cropland expansion (Figure 2a,d,g), CESM and MPI-ESM simulate a quasi-global decrease in evaporation over

all land areas. However, some regions also show an increase such as central U.S. in CESM, as well as East Africa and western

Australia in MPI-ESM. The effects over the mid-latitudes exhibit a strong seasonality, with an increase in evaporation in JJA

255   and a decrease in DJF. This impact is clearly visible in CESM and also slightly visible in MPI-ESM (Figure C1 and Figure

C2). In EC-EARTH, the annual patterns are less clear, with a strong decrease in evaporation following cropland expansion

over tropical forests and a slight decrease over the mid-latitudes, but a clear increase over sub-tropical and tropical regions,

such as the Sahel, East Africa, India and Australia. Moreover, all models clearly distinguish between effects over deforested

grid cells and those that have remained unaltered, following the checkerboard implementation of LCLMC (see Sect. 2.1). In

260   EC-EARTH, there are deforested patches that show a distinct decrease in evaporation while the nearby unaltered grid cells

instead show a strong increase.
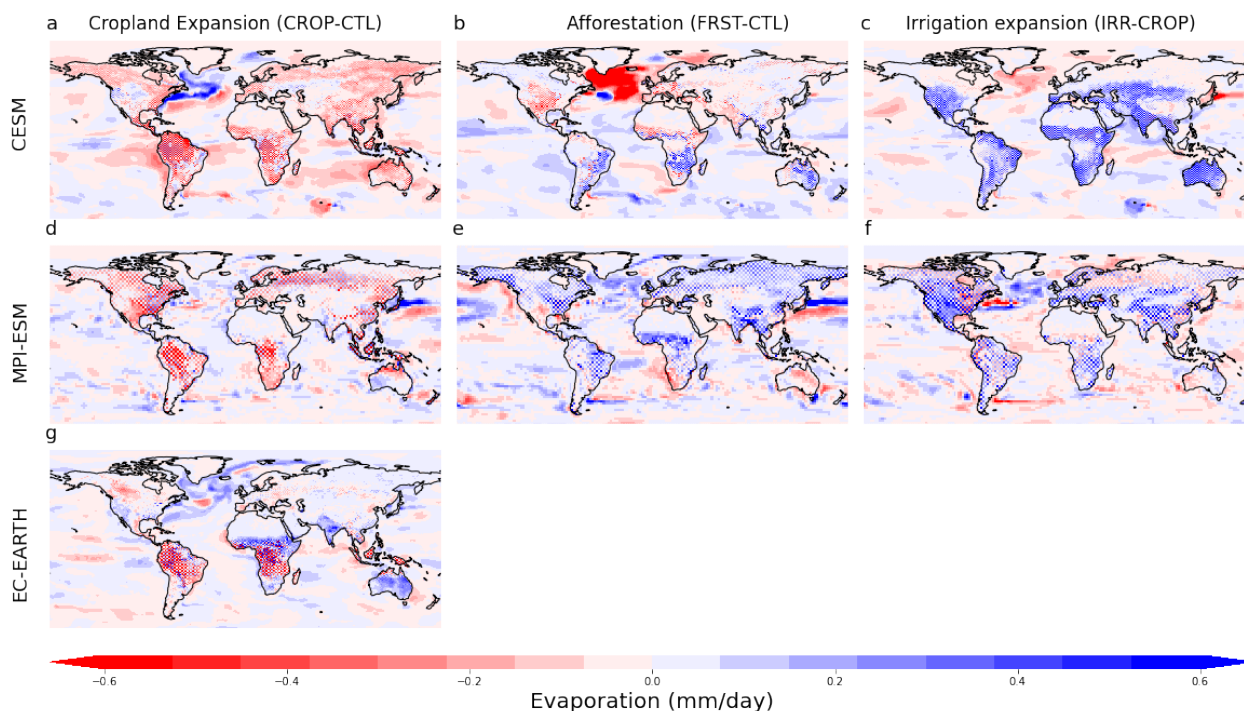
Figure 2. The mean annual impacts of land cover and land management changes on evaporation (mm/day), for cropland expansion (CROP-CTL; a,d), afforestation (FRST-CTL; b,e) and irrigation expansion(IRR-CROP; c,f) for CESM and MPI-ESM respectively. Cropland expansion for EC-EARTH is shown in (g).

Regarding afforestation, MPI-ESM shows opposite patterns compared to cropland expansion, with mostly an increase in

evaporation (Figure 2b,e). However, in CESM this increase is only apparent over the Southern Hemisphere tropics while the

265   Northern-Hemisphere extratropics and the Sahel show a clear increase in annual evaporation due to afforestation. Whereby

it should be noted that the decrease in the extratropics is clearly linked to the boreal summer season (Figure C1 and Figure
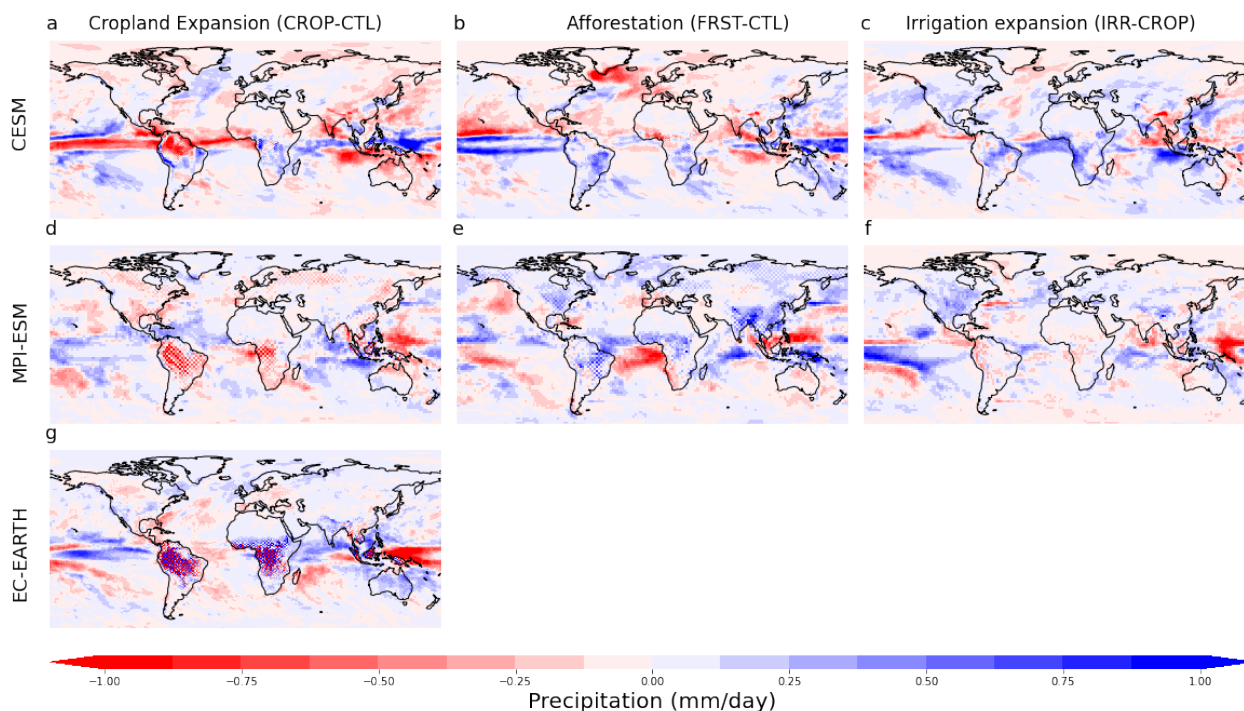
Figure 3. The mean annual impacts of land cover and land management changes on precipitation (mm/day), for cropland expansion (CROP-CTL; a,d), afforestation (FRST-CTL; b,e) and irrigation expansion(IRR-CROP; c,f) for CESM and MPI-ESM respectively. Cropland expansion for EC-EARTH is shown in (g).

C2). Over the North Atlantic, CESM simulates a wide-spread and strong decrease of evaporation, which may be linked to the widespread cooling of the North Atlantic in this ESM (De Hertog et al., 2023). Regarding irrigation expansion, both models, for which this simulation is analysed (CESM and MPI-ESM), strongly agree on the sign of evaporation change over land and simulate a global increase (Figure 2c,f). Differences between both ESMs are mostly related to the extent to which irrigation is applied within the different ESMs (see Figure 1).

The effects of LCLMC on precipitation are less similar across the models, but some regionally consistent patterns emerge (Figure 3). Globally, cropland expansion causes a decrease in precipitation while afforestation and irrigation expansion cause an increase. Under the cropland expansion scenario, there is a decrease of precipitation over land in MPI-ESM (Figure 3b) and CESM, except for Central America, the Congo basin and Eastern Africa (Figure 3a). The patterns of precipitation changes around the tropics in CESM are similar to those found in Portmann et al. (2022). In their study, Portmann et al. (2022) showed that deforestation in CESM is cooling the Northern extratropics, which leads to changes in the intensity of the Hadley cell and the position of the intertropical convergence zone, which could also explain the simulated pattern here. In line with CESM, the cropland expansion simulation with EC-EARTH simulate the largest changes in precipitation over the ocean and forest areas

within the tropics. However, there is a shift of these changes that is causing less precipitation north of Australia and more precipitation over the tropical Pacific. The effects of LCLMCs on MFC also show substantial regional difference between CESM and MPI-ESM (Figure D1). Overall, the patterns in MFC are highly similar to those seen for precipitation (Figure 3) which indicates that these precipitation changes are likely driven by the changes in MFC.

285

Afforestation causes widespread increases in precipitation over land (Figure 3b,e). This increase is quasi-global in MPI-ESM, while in CESM some areas show a precipitation decrease, such as the Indian subcontinent, the Sahel, and Europe. In CESM, the afforestation-induced precipitation differences over the intertropical convergence zone are again similar to those found by Portmann et al. (2022) which indicates that shifts of the large-scale circulation determine the precipitation patterns in
290 this ESM.

For the irrigation expansion scenario, all models simulate a global increase in precipitation. In CESM, it is apparent that Southeast Asia is an exception to this pattern and shows a clear reduction of precipitation despite being an area of large-scale irrigation. This finding might be linked to the hypothesis that the regional temperature decreases as a consequence of irrigation
295 expansion (De Hertog et al., 2023), further causing a weakening of the Indian summer monsoon and a decrease of precipitation over large parts of the continent, a feedback mechanism that has also been documented in previous studies (de Vrese et al., 2016; Guimberteau et al., 2012; Thiery et al., 2017). This decrease in precipitation over India is to some extent also present in MPI-ESM, although it is not as strong as in CESM. However, for both ESMs it is clear that the response over this region occurs mainly during JJA (Figure C3 and Figure C4). This regional decrease is also apparent for MFC (Figure D1c,f), which
300 further supports the weakened Indian Summer Monsoon hypothesis.

3.2 Local and non-local effects on precipitation

The checkerboard implementation allows for a consistent separation between local induced effects, which are directly caused by the LCLMC, and non-local induced effects due to LCLMC elsewhere (See Section 2.1 and Appendix A). In this section
305 we focus on the signal separated results of precipitation for CROP-CTL and IRR-CROP to illustrate this separation in our simulations. The signal separated maps for FRST-CTL and for evaporation are provided in Appendix B.
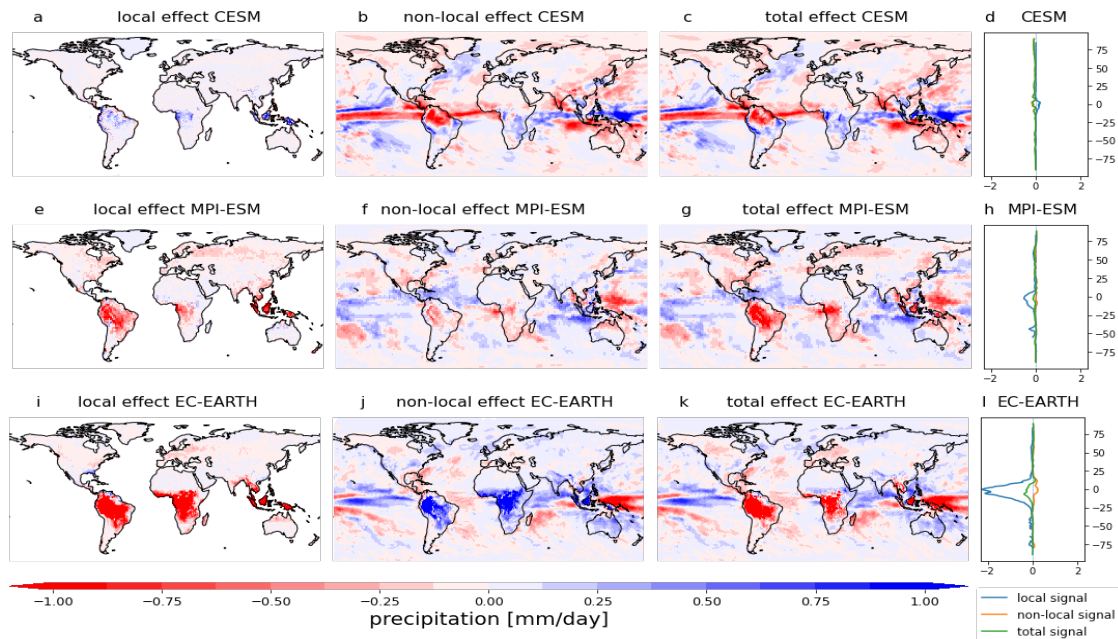
Figure 4. Annual mean precipitation response in mm/day to cropland expansion (CROP-CTL) of CESM, MPI-ESM and EC-EARTH. The local effect in CESM (a), the non-local effect (b) and the total effect (c). The latitudinal average of the local (blue), non-local (yellow) and total (green) signals of CESM (d). (e-h): same as (a-d), but for MPI-ESM. (i-l): same as (a-d), but for EC-EARTH. The stippling on the maps shows grid cells where all the sign of change is consistent throughout the simulation.

Under the cropland expansion scenario, there is a decrease of local precipitation over land in MPI-ESM and EC-EARTH which is especially clear over tropical latitudes (Figure 4e,i). In CESM, in contrast, the majority of the effects are non-local

310 , largely a decrease in precipitation, with only a relatively small local increase in some parts of the tropics. In MPI-ESM the non-local effects shows a regional decrease in precipitation mostly around areas of intense local effects. In EC-EARTH the non-local effects consist of a strong increase of precipitation, countering the local decreases. This is also confirmed by Figure B1 which shows the signal-separated effects of evaporation for the cropland expansion simulations. Using the checkerboard implementation to separate local and non-local effects, EC-EARTH simulates a clear local decrease in evaporation due to crop-

315 land expansion, while the non-local effect cause an increase in evaporation over the tropics, resulting in attenuated total effects (Figure 2). This pattern of strong decreases over areas of LCLMC and decreases in neighbouring grid cells is also visible for $P - E$, used here as proxy for MFC, and indicates a mesocale circulation effects induced by the LCLMC implementation in a checkerboard pattern (see Figure D2g). In both MPI-ESM and EC-EARTH the local effects dominate the total signals while for CESM the total signal is mostly determined by the non-local effects. This further indicates that the results in CESM appear

320 to be dominated by circulation changes which is also apparent in the signal separated results for afforestation (Figure B4).
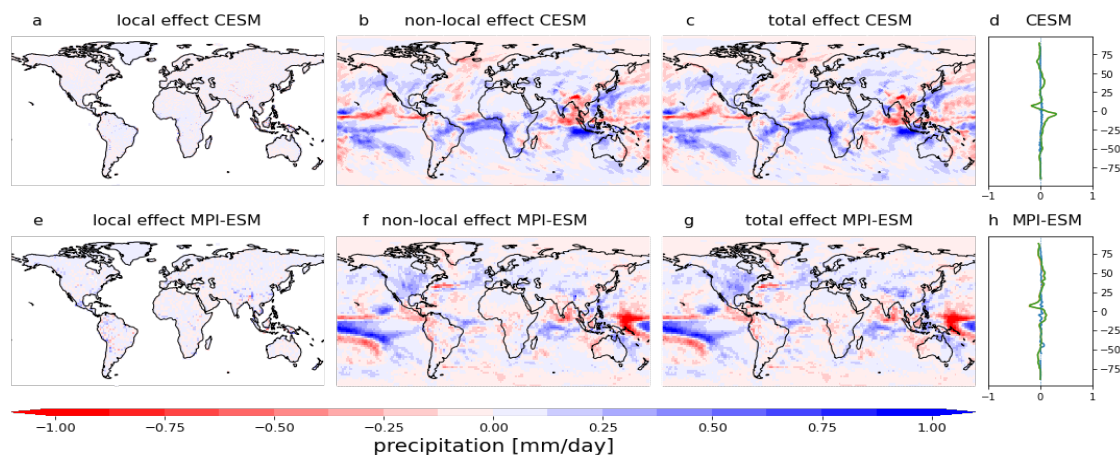
Figure 5. Annual mean precipitation response in mm/day to irrigation expansion (IRR-CROP) of CESM and MPI-ESM. The local effect in CESM (a), the non-local effect (b) and the total effect (c). The latitudinal average of the local (blue), non-local (yellow) and total (green) signals of CESM (d). (e-h): same as (a-d), but for MPI-ESM. The stippling on the maps shows grid cells where all the sign of change is consistent throughout the simulation.

For irrigation expansion, both MPI-ESM and CESM indicate a dominant non-local increase in precipitation (Figure 5) which is mostly apparent in regions of intense irrigation (Figure 1). In MPI-ESM there are some smaller local increases in precipitation as well while in CESM the local effect appears unimportant. This general pattern does not hold over India where both

325 ESMs show a non-local decrease in precipitation over this region despite a strong local increase in evaporation (Figure B3) which indicates that circulation patterns are dominantly driving this effect. These signal separated results help in characterising the effects on the atmospheric water cycle within the different ESMs. However, they do not provide any information on the effects on moisture recycling which is analysed using the WAM-2layer moisture tracking algorithm in the next section.

330 **3.3 Changes in local precipitation and evaporation length scales due to LCLMC**

To unravel the direct impact of LCLMC-induced evaporation changes on the precipitation over land (and the other way around), we evaluate the outputs from WAM-2layers and illustrate local evaporation and precipitation length scales for each model and LCLMC scenario. An overview of consistent patterns for change in moisture fluxes and length scales is shown in Table 1. Even in their control simulations, the different ESMs show very different magnitudes of length scales of moisture recycling, both

335 for the precipitation length scale (Figure 6) and the evaporation length scale (Figure 7). CESM shows the largest length scales indicating that the importance of local recycling is relatively small. EC-EARTH, in contrast, generally shows very low values of the length scale indicating that local recycling is more important within this ESM. The length scale values captured by the three ESMs in our study lie within the broad range of values found in literature (van der Ent and Savenije, 2011; Theeuwen et al., 2023), even if the results are not directly comparable as they are based on reanalysis data. To our knowledge, no studies

340   exist presenting length scales for ESMs. However, it is known that ESMs simulate substantial differences in the global water
cycle (Li et al., 2022), which logically also translates to substantial differences in length scales. Both reanalysis-based studies
(van der Ent and Savenije, 2011; Theeuwen et al., 2023, e.g.) present values for the length scales ranging roughly within 1000-
7000 km for the majority of the land surface. In general, CESM overestimates the length scales compared to literature while
EC-EARTH shows values at the lower end. Yet, the spatial patterns are quite similar among the ESMs and comparable to those

345   in literature (van der Ent and Savenije, 2011; Theeuwen et al., 2023). The precipitation length scale is smallest over tropical
rainforests and mountain ranges (see for example the Tibetan Plateau) indicating that these locations mostly get precipitation
from nearby evaporation. These patterns also occur for the evaporation length scale, although here locations with a dry and
continental climate such as Siberia and Western North America also show very low values. This implies that evaporation oc-
curring within these locations generally precipitates nearby.

350
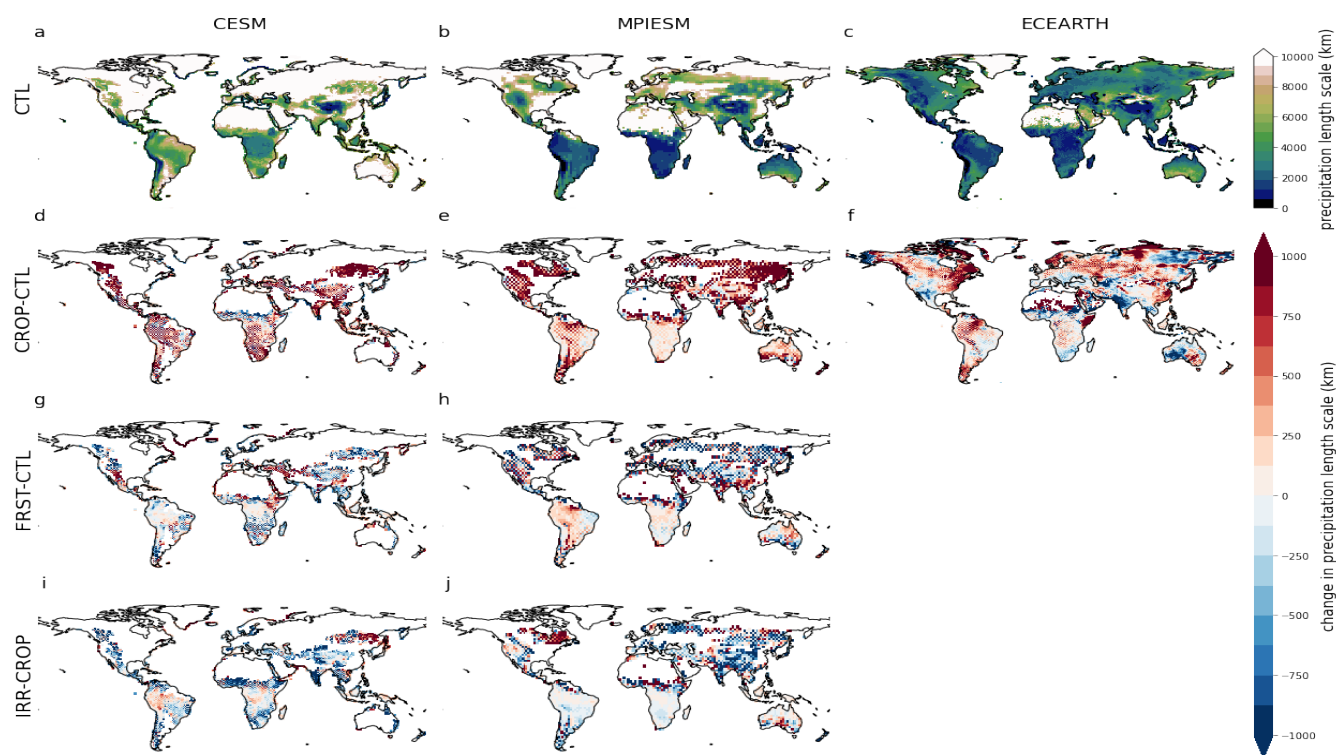
Figure 6. The annual mean precipitation length scale (km) for the control (CTL) simulation in CESM (a), MPI-ESM (b) and EC-EARTH
(c). The effect of cropland expansion (CROP-CTL) on the annual mean precipitation length scale is shown for CESM (d), MPI-ESM (e)
and EC-EARTH (f). The effect of afforestation (FRST-CTL) is shown for CESM (g) and MPI-ESM (h) and finally the effect of irrigation
expansion (IRR-CROP) is shown for CESM (i) and MPI-ESM (j). Note that in the difference plots in (d)–(j), the areas with a reference
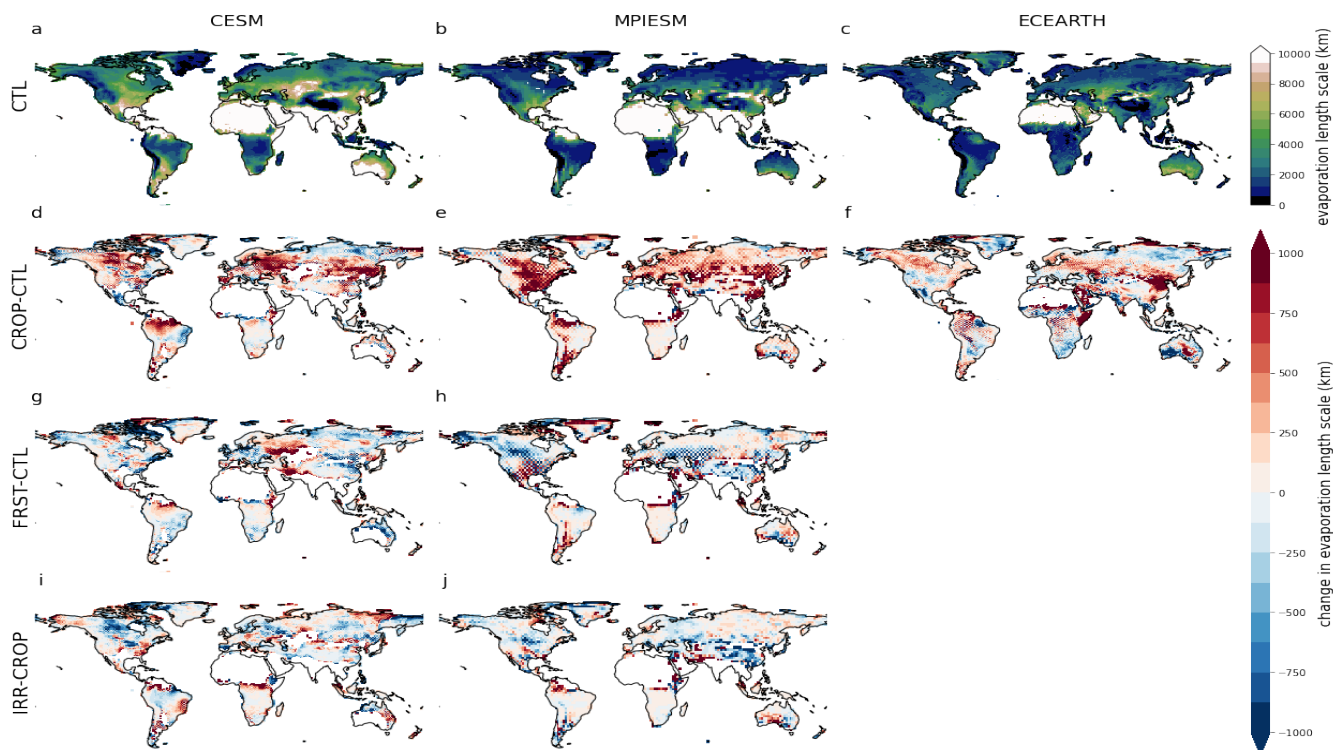evaporation length scale higher than 10000 km are cropped out.

15

Figure 7. The annual mean evaporation length scale (km) for the CTL simulation in CESM (a), MPI-ESM (b) and EC-EARTH (c). The effect of cropland expansion (CROP-CTL) on the annual mean evaporation length scale is shown for CESM (d), MPI-ESM (e) and EC-EARTH (f). The effect of afforestation (FRST-CTL) is shown for CESM (g) and MPI-ESM (h) and finally the effect of irrigation expansion (IRR-CROP) is shown for CESM (i) and MPI-ESM (j). Note that in the difference plots in (d)–(j), the areas with a reference precipitation length scale higher than 10000 km are cropped out.

In general, both the precipitation and evaporation length scale increase as a consequence of cropland expansion (see Figures 6d,e,f and 7d,e,f). In MPI-ESM, it seems that the Congo Basin is an exception with no clear changes in local recycling occurring there. In EC-EARTH, the patterns are more blurred than in the other ESMs with a decrease in length scales in some regions, such as South Africa and spots over the Central U.S. . However, over regions where the largest cropland expansion occurred (such as Amazon basin and China, see also Figure 1), the patterns are consistent with the other ESMs. Over Latin America, a dipole pattern of the change in the evaporation length scale in both EC-EARTH and CESM appears, showing an increase in the West and a decrease in the East. The general increase in length scale due to cropland expansion implies that the LCLMC induces a decrease in local recycling.

Afforestation (Figures 6g,h and 7g,h), induces a pattern that is opposite to the cropland expansion case, with a decrease in length scale for both precipitation and evaporation. However, in some areas, the patterns diverge from the general trend, e.g. afforestation causes an increase of the evaporation length scale over the Amazon in CESM, and an increase of the precipitation

Table 1. Summary of the effects of moisture fluxes over land due to the different LCLMC. Each cell indicates where the changes in moisture response are consistent in sign.

LCLMC	E	P	λ_ϵ	λ_ρ
CROP-CTL	decrease over tropics	regional increase/decrease	mostly decrease	mostly increase
FRST-CTL	increase over tropics	increase over tropics	global increase	mostly decrease
IRR-CROP	global increase	global increase	global decrease	global decrease

length scale over the tropics in MPI-ESM. In general, the changes in both length scales are stronger for the extratropics, which is particularly visible for the evaporation length scale. This effect on the evaporation length scale may be explained by the fact

365 that the tropics are already densely forested in the CTL scenario and thus the additional trees do not alter the local recycling favouring conditions, in contrast to the sparsely forested extratropics (Figure 1).

Regarding irrigation expansion (Figures 6i,j and 7i,j), the effects on the evaporation length scale are less clear and generally of small magnitude. Irrigation-induced differences show a tendency towards a decreased evaporation length scale, which is

370 rather consistent in MPI-ESM but in CESM this pattern is less clear. The effects on the precipitation length scale in both ESMs are larger and more consistently decreasing due to irrigation expansion. The change in precipitation length scale is small over the tropics due to the small amount of irrigation applied in this region (Figure 1). We even observe a slight increase in length scale over the tropical forest in CESM and over some areas in the U.S. in MPI-ESM, which might imply circulation changes in those regions.

375 **3.4   Changes in continental moisture recycling due to LCLMC**

While there are substantial differences in the local effects of LCLMC on the water cycle, their net impact on water availability over land might be the same. Here, we evaluate how LCLMC impacts E, P and P-E over land, and we identify the direct impact of LCLMC-induced effects on these fluxes via continental moisture recycling (see Section 2.3.4). The values of total annual precipitation (P), continental precipitation (Pc), continental precipitation recycling (ρ_c), evaporation (E), continental evapo-

380 ration (Ec) and continental evaporation recycling (ϵ_c) are included in Appendix E. Cropland expansion causes a net decrease of evaporation from land in CESM and MPI-ESM, while EC-EARTH simulates a small net increase of continental evaporation (Figure 8a). Through this decrease of evaporation in CESM and MPI-ESM, less moisture is available for continental moisture recycling (dark bars in Figure 8a) and for precipitation over oceans (light bars in Figure 8a). Analogously, cropland expansion is causing a net decrease of precipitation over land in CESM and MPI-ESM, but a net increase in EC-EARTH, which is due

385 to contrasting signs of change in different parts of the globe (Figure E2). In the former two models, the simulated decrease of precipitation mainly results from decreased moisture imports from the ocean (light bars in Figure 8b), and only 42% and 26% respectively of the precipitation deficit is estimated to be of continental origin (dark bars in Figure 8b).

The effects on evaporation from land due to afforestation are consistent in sign and generally cause an increase for both ESMs. A large part of this increase is available for continental moisture recycling (dark bars in Figure 8a) in CESM (48%),

390 but is negligible for MPI-ESM (2%). In MPI-ESM the increase in land evaporation mainly rains out over the oceans (light bars in Figure 8a). Evaluated over all land regions, afforestation increases precipitation over land in both MPI-ESM and CESM Figure 8b). The magnitude is much smaller in CESM due to the large spatial heterogeneity in precipitation effects (Figure E1), which cancel each other out causing only a small net increase of precipitation over land. For MPI-ESM, there is a large heterogeneity within the signal of change (Figure E1), causing diverging contributions of moisture for continental precipitation from

395 ocean and land. Atmospheric circulation changes in this model cause an increase in precipitation of oceanic origin on land, while less precipitation is estimated to be of continental origins.

Regarding irrigation expansion, there is a strong increase of evaporation from land in CESM, of which most rains out over the oceans (light bar in Figure 8a), and only a small fraction (17%) is available for continental moisture recycling (dark bar in

400 Figure 8a). In MPI-ESM, the effect is smaller due to some areas of decreased recycling (Figure E2) but the results still show an overall increase in evaporation of which most rains out over the ocean. For precipitation over land, the effect is not consistent across the ESMs. In CESM there is an increase in precipitation over land of which 34% is available for continental recycling. In contrast, for MPI-ESM there is a global decrease of continental precipitation, of which 12% stems from the precipitation deficit over land.
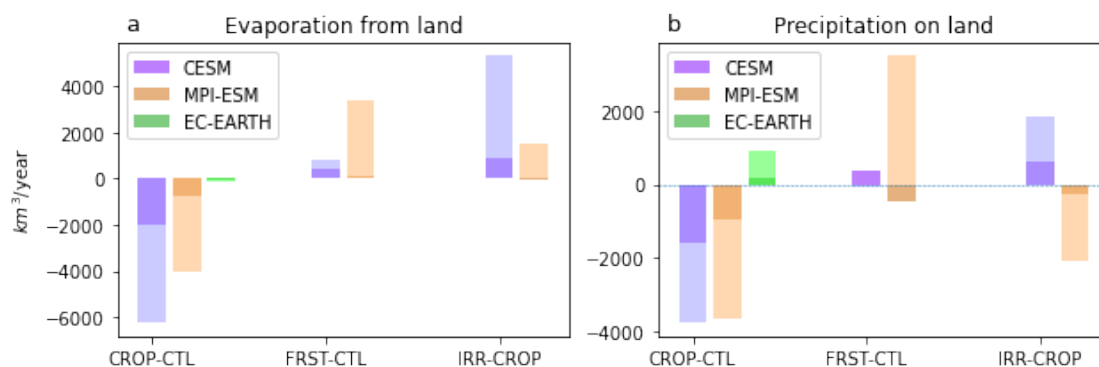
405

Figure 8. The global change in annual mean evaporation (a) and precipitation (b) on land is shown for CESM in blue, MPI-ESM in orange and EC-EARTH in green for cropland expansion (CROP-CTL), afforestation (FRST-CTL) and irrigation expansion (IRR-CROP). The contribution of continental moisture recycling changes is shown in a darker shade of the ESMs respective colours.
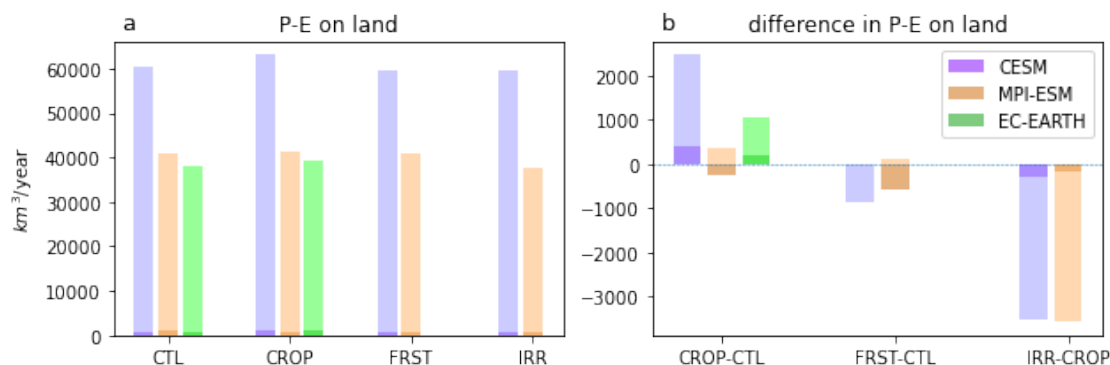
Figure 9. The total annual mean P-E on land (a) and change in P-E on land (b) is shown for CESM in blue, MPI-ESM in orange and EC-EARTH in green for cropland expansion (CROP-CTL), afforestation (FRST-CTL) and irrigation expansion (IRR-CROP). The contribution of continental moisture recycling changes is shown in a darker tone of the ESMs respective colours.

Finally, we can quantify the global effects of LCLMC on global water exports from land towards the ocean by analysing the effects on P-E. In general, $P - E$ is positive for all three ESMs, being substantially larger in CESM than in MPI-ESM and EC-EARTH (Figure 9a), indicating that the land receives more water from the atmosphere, and of oceanic origin, than it provides through evaporation. Both evaporation and precipitation decreases for MPI-ESM and CESM due to cropland expansion

410 (Figure 8), but the decrease in evaporation is larger causing a net surplus of water at the land surface (i.e., $\Delta(P - E) > 0$). There is also a net surplus of water for EC-EARTH although this is mostly due to increased continental precipitation (Figure 8). In EC-EARTH and CESM, the contribution due to continental recycling is 16% and 20% respectively (light bars in Figure 8 and Figure 9b), but the majority comes from changes in oceanic moisture. This differs from MPI-ESM, where less moisture is recycled (dark bar in Figure 9b). Afforestation, in turn, is causing a net loss of water at the land surface for both ESMs.

415 CESM simulates an increase in water export from land through an increase of land evaporation that rains out over the ocean (Figure 9b). In contrast MPI-ESM shows a slight increase in water availability over land due to oceanic moisture, with the effect of continental moisture changes dominating the global decrease in water availability. Following irrigation expansion, both CESM and MPI-ESM simulate a decrease in water available on land. In both simulations, enhanced evaporation through irrigation from land (see Figure 8a) mostly rains out over the ocean (light bars in Figure 9b), thus a loss of water on land to the

420 ocean with the contribution of continental recycling being 8% and 5% for CESM and MPI-ESM, respectively.

4   Discussion

LCLMC can have substantial effects on atmospheric moisture fluxes and the local and continental recycling of moisture that determine water availability on land. Common patterns emerge from our multi-model analysis, despite strong differences in the implementation of LCLMC and the simulation of the hydrological response in the different ESMs. For cropland expansion,

425 all three ESMs agree that there is a general decrease over land in evaporation and precipitation over most regions as well

as a decreased local recycling strength. In contrast, afforestation and irrigation expansion show an opposite pattern of both increased precipitation and evaporation over most regions with enhanced local recycling strength. Here we will discuss some of the discrepancies between the different ESMs and their implications on moisture fluxes and moisture recycling.

4.1 Different hydroclimatic responses of ESMs to LCLMC

430 The effects of LCLMC within the different ESMs have strong regional variations (e.g., Figure 2 and Figure 3). The differing length scales between ESMs (Figure 7 and Figure 6) illustrate that different processes dominate within the different ESMs: EC-EARTH shows a stronger importance of local processes in contrast to CESM, where atmospheric circulation seems to dominate the effects. This is also illustrated through the signal separated results (Figure 4 and 5) where CESM mainly shows non-local effects, while MPI-ESM and EC-EARTH show a stronger importance of local effects. This difference is also clear

435 from the effects on moisture fluxes as EC-EARTH simulates strong mesoscale effects (10 to 100 km), while in CESM global circulation changes appear to dominate. CESM is known to be an ESM with a strong natural variability, as was shown in several other studies (Deser et al., 2012, 2020). It has also been shown to simulate large-scale circulation shifts as a consequence to land cover change (Portmann et al., 2022; Devaraju et al., 2018).

440 Discrepancies in the CTL length scales estimated for each ESM could also stem from the different spatial resolutions employed here (CESM:0.90°x1.25°, MPI-ESM:1.88°x1.88° and EC-EARTH:0.7°x0.7°). Although the concept of length scales is independent of the spatial resolution (van der Ent and Savenije, 2011), the capability of ESMs to resolve processes explicitly is resolution-dependent. This implies that certain processes, such as mesoscale convection, are potentially better resolved within EC-EARTH than in CESM and MPI-ESM. These strong differences in length scales, despite showing effects from induced

445 LCLMC on local length scales which are consistent in sign, are important as they clearly illustrate some of the challenges involved in modelling the atmospheric water cycle using ESMs. The LCLMC effects on climate simulated by CESM are dominated by circulation effects with less importance of moisture recycling than a world as simulated by EC-EARTH. A next step to better understand these strong differences could be to evaluate the outputs of ESMs to reanalysis products in order to better understand potential biases in evaporation and precipitation fluxes that could help in explaining these differences.

450 The way LCLMC is implemented in the different ESMs also causes some discrepancies. Some of the ESMs only represent crops by few generic crop types (such as MPI-ESM) while others have different crop types representing different biophysical properties. CESM has eight different crop types representing common crops around the world (Lombardozzi et al., 2020). In CESM, maize has high evaporation rates which might explain why afforestation over the Northern Hemisphere extratropics

455 is causing a decrease in evaporation, with particularly strong effects during summer Figure C1. The discrepancy between the effects due to afforestation and cropland expansion can be partially explained by a saturation effect, as the effects of adding trees are likely non-linear (Winckler et al., 2017b). For example, in the tropics, extreme deforestation will have larger impacts on the hydrological cycle than adding trees in an already densely forested region. This effect could explain some differences

between these simulations such as the smaller precipitation length scale changes in afforestation over the tropics.

460

The implementation of irrigation also causes substantial differences in climatic responses among the ESMs, as the maps of irrigation extent and amounts differ strongly (Figure 1). Both MPI-ESM and CESM show an increase in precipitation, except for the Indian subcontinent where both ESMs show a decrease in precipitation. As there is a cooling over all irrigated areas (De Hertog et al., 2023), there is a lower land–ocean temperature contrast, which reduces convection over land and therefore

465 precipitation (Figure 3 and Figure D1). This occurs despite the increases in evaporation (Figure 2) and enhanced local precipitation recycling (Figure 6). Considering all the above, it is likely that the reduced precipitation shown here is caused by a weakened Indian Summer Monsoon as was highlighted by previous studies (Puma and Cook, 2010; de Vrese et al., 2016; Thiery et al., 2017, 2020).

470 ## 4.2 Implications of changes in moisture recycling due to LCLMC

LCLMC strongly affects the redistribution of moisture over land in the ESMs. While the absolute length scales of moisture recycling differ among the ESMs, LCLMC-induced changes are consistent across the ESMs, with cropland expansion causing decreased recycling and afforestation and irrigation expansion mostly causing enhanced local recycling (Figure 7 and Figure 6). The effects of LCLMC on continental recycling and the continental contribution to precipitation over land and evaporation from

475 land are less consistent across ESMs (Figure 8 and Figure 9), but also geographically more heterogeneous within the ESMs (Figure E1 and Figure E2). This is due to the complex interactions of local effects with non-local effects, such as advection and circulation changes, which all affect the redistribution of water globally.

Although the effects of LCLMC on the precipitation and evaporation changes are substantial, they are not as large as could

480 be expected based on literature (Tuinenburg et al., 2020; Hoek van Dijke et al., 2022; Baudena et al., 2021; Wunderling et al., 2022; Staal et al., 2018). This could partially be due to the less extensive LCLMC scenarios considered here (only 50% change due to checkerboard approach). However, differences are expected because most previous studies are based on reanalyses and can only estimate the impact of upwind LCLMC changes on downwind precipitation using constant recycling ratios, neglecting any other interactions. Therefore, to fully capture the impact of LCLMC on moisture recycling, LCLMC model simulations

485 should be compared to a control simulation, as done here. In fact, the resulting (substantial) differences in recycling ratios show that the interactions that are not considered when basing the studies on reanalysis are not negligible. As LCLMC becomes increasingly relevant as a climate mitigation strategy it is important to consider a more holistic view of the influence of these strategies on the water cycle. Consequently, more research is needed to better constrain the effects of LCLMC on moisture recycling, aiming to support science that can guide future land cover planning.

490

4.3 Circulation effects induced by checkerboard LCLMC implementation

The specific setup of these simulations, with a checkerboard pattern LCLMC, also has limitations and causes some artefacts within the results. This is, for example, illustrated in the clear checkerboard pattern visible for evaporation (Figure 2) and precipitation changes (Figure 3) from EC-EARTH, especially over the tropics. Due to the area dependence of the effects of

495   land cover changes on moisture fluxes (Spracklen et al., 2018), mesoscale circulation effects occur in EC-EARTH but do not appear in the other (coarser) ESMs (see for example Figure 4). This checkerboard-like effect would likely not occur if a full land cover change was simulated instead of the checkerboard implementation of the LCLMC. This implementation could have some important implications, as the non-local effects for EC-EARTH do not represent the effects one would get in a full land cover change simulation, implying that the assumptions behind the checkerboard approach are not met (Winckler

500   et al., 2017a; De Hertog et al., 2023). Moreover, the LCLMC-induced effects on atmospheric circulation and moisture fluxes also affect other climate variables, such as temperature. These checkerboard-induced circulation changes could also explain the differences between the temperature effects found in De Hertog et al. (2023): here, the checkerboard-implementation of cropland expansion in EC-EARTH caused tropical warming, and the simulations from Boysen et al. (2020) with EC-EARTH that simulated full deforestation changes (forest to grass conversion), showed tropical cooling. Further research is

505   required to completely understand the implications of checkerboard-induced climate effects. For example, the LCLMC could be implemented in different densities (1/8, 1/4, 1/2) next to a full deforestation experiment to assess whether these effects are true artefacts of the LCLMC patterns. However, this might imply that the checkerboard approach for signal separation requires a rough spatial implementation to avoid mesoscale circulation effects as seen here for EC-EARTH.

5 Conclusions

510   In this study, we analysed the effects of land cover and land management changes (LCLMC) on the atmospheric water cycle in a slate of idealised simulations (cropland expansion, afforestation and irrigation expansion) performed by three different Earth System Models (ESMs). We showed that the effects on moisture fluxes are substantial with, generally, decreased evaporation and precipitation over land due to cropland expansion and the opposite effects for afforestation and irrigation expansion. However, substantial discrepancies between the different ESMs exist, with EC-EARTH displaying important local recycling and

515   mesoscale circulation effects, while CESM shows a dominance of large-scale atmospheric circulation shifts. These differences can have various causes, such as model parameterisations of crucial processes (e.g., convection) or the extent to which different land cover types are implemented within the ESMs on a global scale. Because some of these effects might have been indirectly influenced by the checkerboard LCLMC pattern used in this study, we advocate for more research to assess the implications of possible checkerboard-induced climate effects and the applicability of this approach for signal separation into local and non-

520   local effects. Despite the strong differences between ESMs, the effects on local recycling are generally consistent in sign, with cropland expansion causing a decreased recycling strength, and afforestation and irrigation expansion generally causing an increased recycling strength. Overall we find that cropland expansion causes a net increase in water availability on land while afforestation and irrigation expansion cause a net decrease. Our simulations show that changes due to atmospheric circulation

Earth System
Dynamics
Discussions

525 patterns play an important role in explaining these patterns and should be taken into account when assessing the effects of LCLMC on moisture recycling.

This is the first study – to our knowledge – to explicitly consider moisture recycling when assessing the LCLMC effects on moisture fluxes using multiple ESMs. Our results show that the effects of LCLMC on moisture recycling are substantial both on the local and global scale, with clear implications for water availability on land. The potential effects of LCLMC on the
530 atmospheric water cycle should therefore be considered in future land cover planning.

Code and data availability. The scripts used for the analysis of the moisture fluxes and the adapted version of WAM-2layers can be found on the GitHub page of the Department of Hydrology and Hydraulic Engineering of VUB (https://github.com/VUB-HYDR/2023_DeHertog_etal_ESD). The simulation data and postprocessed data used in this paper are available through dkrz (https://www.wdc-climate.de/ui/entry?acronym=DKRZ_LTA_1147_ds00003).

535 **Appendix A: Summary of checkerboard approach for signal separation**

The checkerboard approach was developed by Winckler et al. (2017a) for the signal separation into local and non-local effects within dedicated simulations with the MPI-ESM. Subsequently it has been applied to the LCLMC simulations performed within the LAMACLIMA project in a multi-model framework (De Hertog et al., 2023). 'Local effects' are defined as the direct climate effect due to the changes in land surface properties within a given grid cell. While 'non-local effects' are climate effects
540 caused by changes in atmospheric circulation or advection as a consequence of LCLMC elsewhere (Winckler et al., 2017a). Here we summarise the approach and highlight technical processing steps taken to extract the local and non-local signal from the raw ESM output.

The checkerboard approach allows a robust signal separation of local and non-local effects by implementing the LCLMC in a checkerboard pattern, i.e. alternating 'change' grid cells, where LCLMC occurs, with 'no change' grid cells, which retain the
545 CTL land cover (see Figure 1). It can then be assumed that any effects in climate variables over the 'no change' grid cells can be attributed as a non-local effect while in the 'change' grid cells of the raw model output both local and non-local effects occur (Winckler et al., 2017a). The 150 year-simulation with constant external forcings is split into 5 slices of 30 years each. To account for natural variability, we treat each slice as a member of a perturbed initial condition ensemble. In order to apply the signal separation, a multi-year monthly mean is computed over each of these ensemble members (De Hertog et al., 2023).
550 (1) We subtract a reference member from the LCLMC member of interest, i.e., for CROP and FRST this reference member is CTL while for the IRR simulation it is CROP. (2) We mask the LCLMC grid cells of this difference map, hence, retaining only those grid cells where only non-local effects occur. (3) The grid cells with only non-local effects are spatially interpolated to fill the masked LCLMC grid cells in order to create a global map of the non-local effect. Consequently, to create a global map of the local effects, we mask all 'no change' grid cells from the difference map created in (1), thus only retaining the grid cells

where both local and non-local effects occur. The values of these grid cells are then corrected by the interpolated non-local values in order to only retain the local effects. Subsequently, the values of the resulting grid cells are again spatially interpolated in order to attain a full global map of local effects. Finally, the sum of both, the local and non-local effects, then represents the total effect. This is the effect we would expect if an actual idealised LCLMC simulation had been performed without an LCLMC checkerboard pattern, although it should be noted that this total effect can be considered a lower limit as the non-local effects represent only a 50% change simulation (Winckler et al., 2017a). The checkerboard approach is implemented to each model grid at its native resolution. Hence, grid cell sizes vary across the different ESMs. As we have five ensemble members of 30 years for each simulation, we can extract local and non-local signals for each ensemble member, which are then used as a measure of uncertainty coming from natural variability (De Hertog et al., 2023). Within this study we focus on interpreting the raw ESM output (as this is used in the moisture tracking analysis) and only apply the signal separation for completeness and to support the interpretation of the presented results.

Appendix B: Signal separated plots of evaporation and precipitation
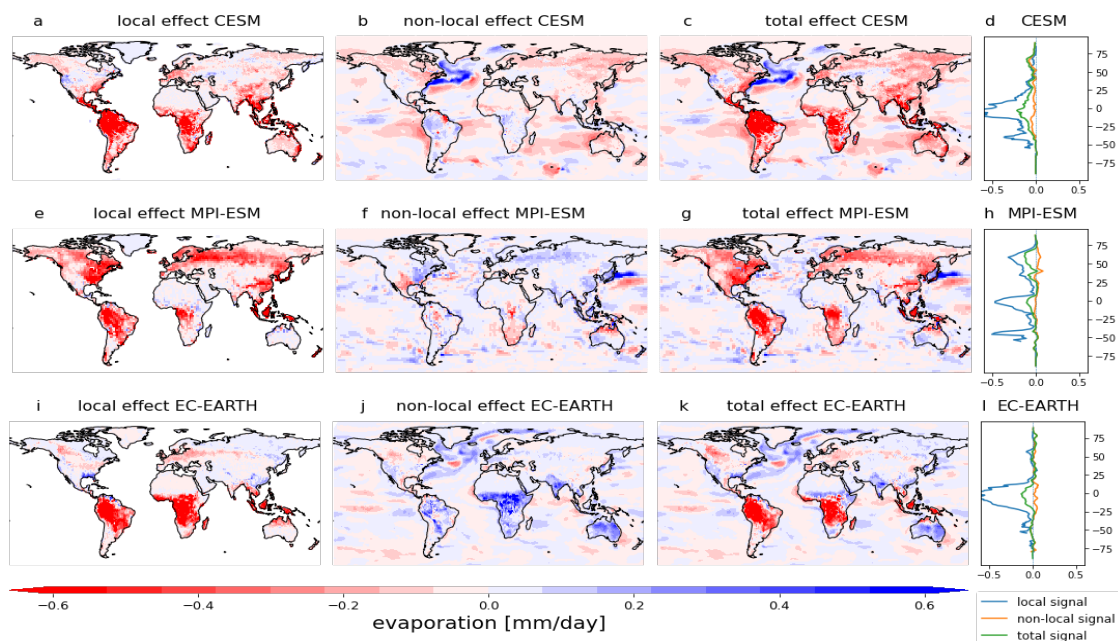
Figure B1. Annual mean evaporation response in mm/day to cropland expansion (CROP-CTL) of CESM, MPI-ESM and EC-EARTH. The local effect in CESM (a), the non-local effect (b) and the total effect (c). The latitudinal average of the local (blue), non-local (yellow) and total (green) signals of CESM (d). (e-h): same as (a-d), but for MPI-ESM. (i-l): same as (a-d), but for EC-EARTH. The stippling on the maps shows grid cells where all the sign of change is consistent throughout the simulation.
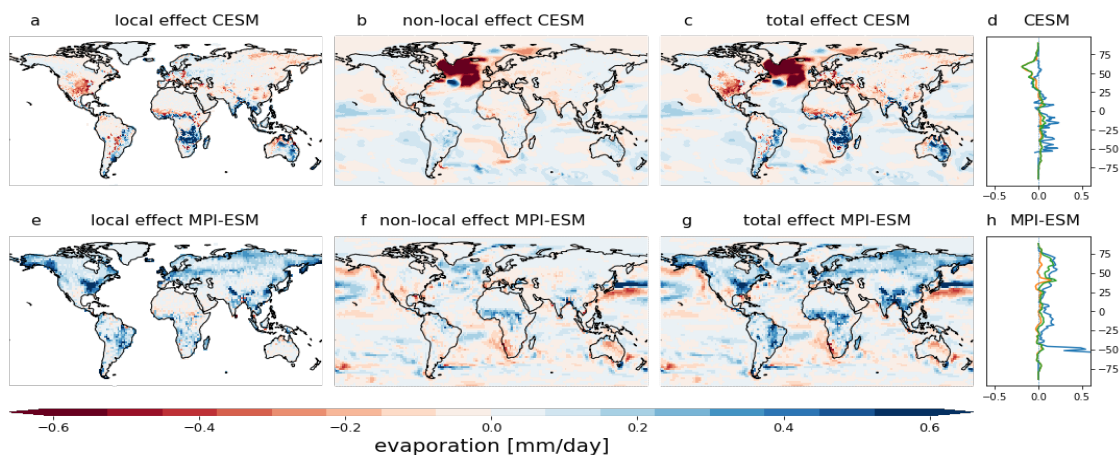
Figure B2. Annual mean evaporation response in mm/day to afforestation (FRST-CTL) of CESM and MPI-ESM. The local effect in CESM (a), the non-local effect (b) and the total effect (c). The latitudinal average of the local (blue), non-local (yellow) and total (green) signals of CESM (d). (e-h): same as (a-d), but for MPI-ESM. The stippling on the maps shows grid cells where all the sign of change is consistent throughout the simulation.
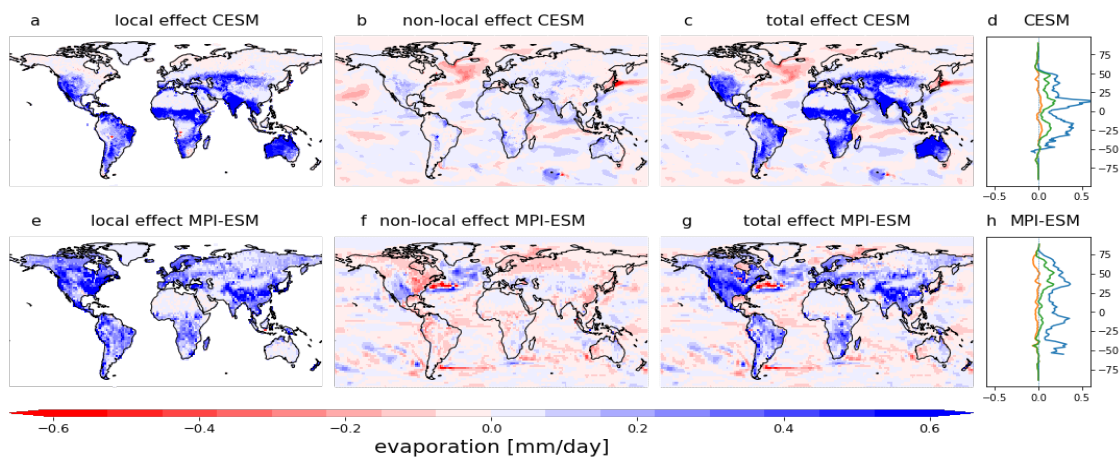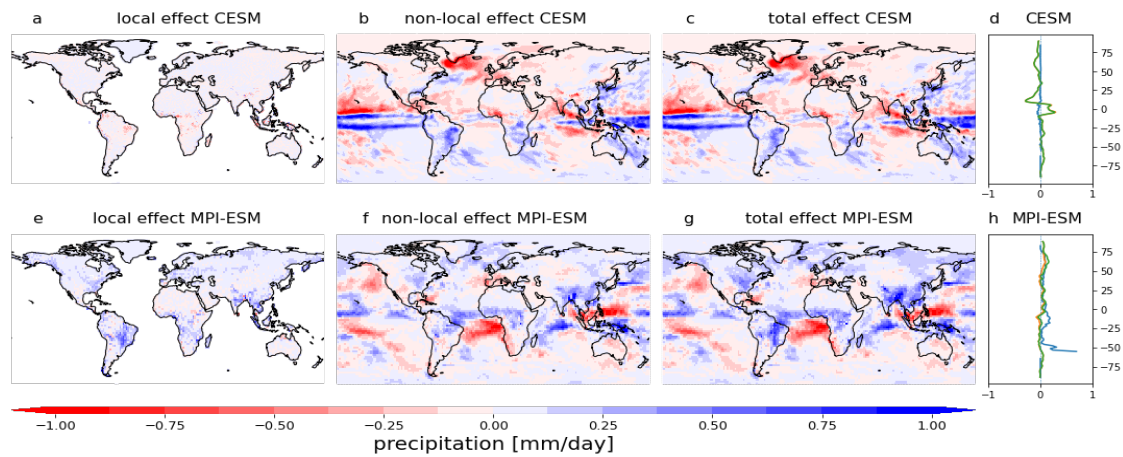

Figure B3. Annual mean evaporation response in mm/day to irrigation expansion (IRR-CROP) of CESM and MPI-ESM. The local effect in CESM (a), the non-local effect (b) and the total effect (c). The latitudinal average of the local (blue), non-local (yellow) and total (green) signals of CESM (d). (e-h): same as (a-d), but for MPI-ESM. The stippling on the maps shows grid cells where all the sign of change is consistent throughout the simulation.

Figure B4. Annual mean precipitation response in mm/day to afforestation (FRST-CTL) of CESM and MPI-ESM. The local effect in CESM (a), the non-local effect (b) and the total effect (c). The latitudinal average of the local (blue), non-local (yellow) and total (green) signals of CESM (d). (e-h): same as (a-d), but for MPI-ESM. The stippling on the maps shows grid cells where all the sign of change is consistent throughout the simulation.

Appendix C: Seasonal effects on evaporation and precipitation
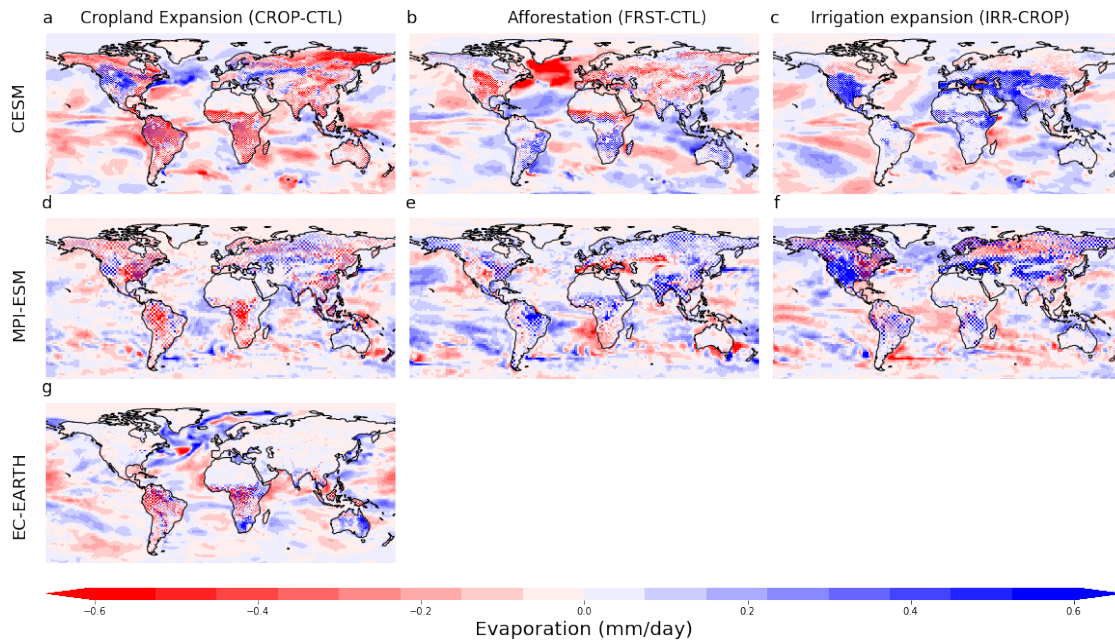
Figure C1. The seasonal mean (JJA) effects on evaporation in mm/day as a consequence of cropland expansion (CROP-CTL) in CESM (a), MPI-ESM (d) and EC-EARTH (g), for afforestation (FRST-CTL) in CESM (b) and MPI-ESM (e) and irrigation expansion (IRR-CROP) for CESM (c) and MPI-ESM (f).
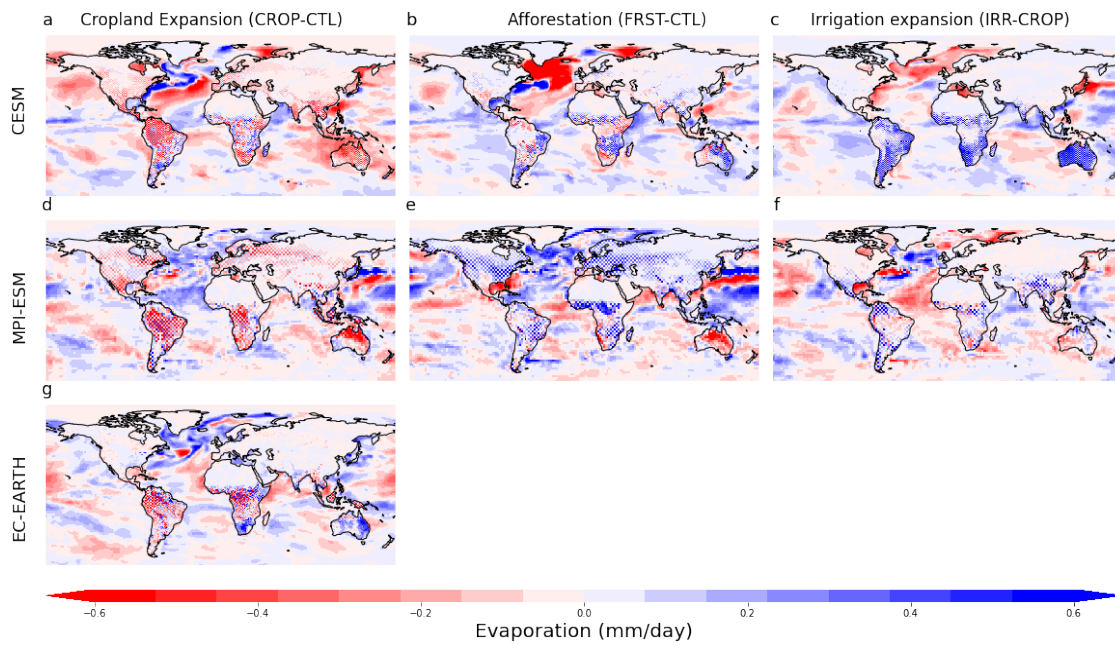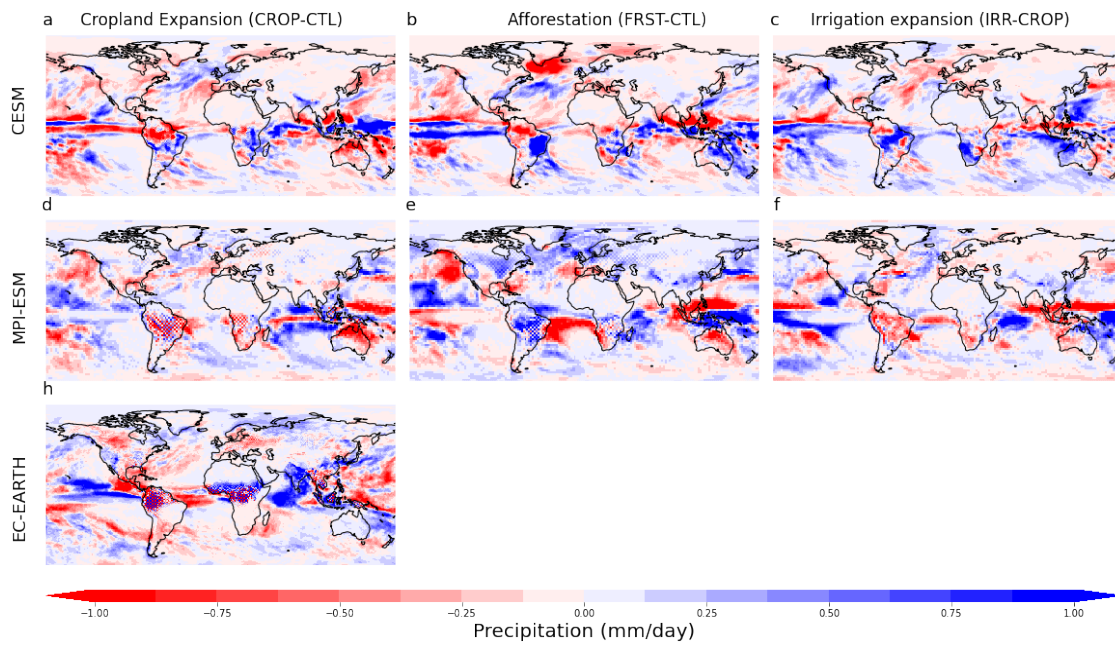
Figure C2. The seasonal mean (DJF) effects on evaporation in mm/day as a consequence of cropland expansion (CROP-CTL) in CESM (a), MPI-ESM (d) and EC-EARTH (g), for afforestation (FRST-CTL) in CESM (b) and MPI-ESM (e) and irrigation expansion (IRR-CROP) for CESM (c) and MPI-ESM (f).
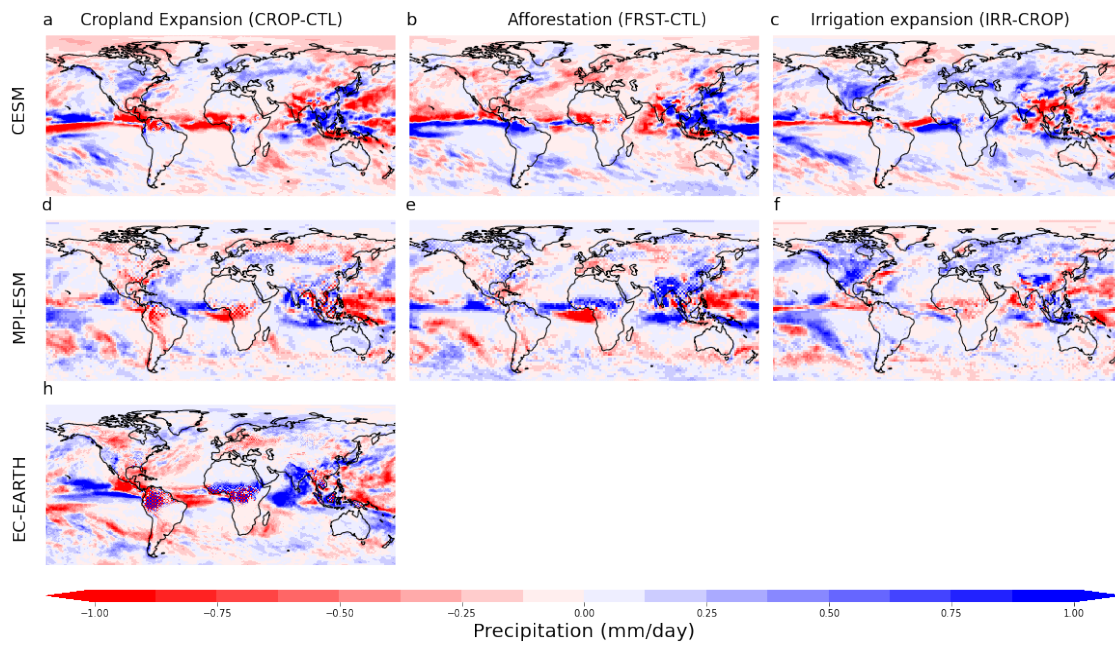
Figure C3. The seasonal mean (JJA) effects on precipitation in mm/day as a consequence of cropland expansion (CROP-CTL) in CESM (a), MPI-ESM (d) and EC-EARTH (g), for afforestation (FRST-CTL) in CESM (b) and MPI-ESM (e) and irrigation expansion (IRR-CROP) for CESM (c) and MPI-ESM (f).
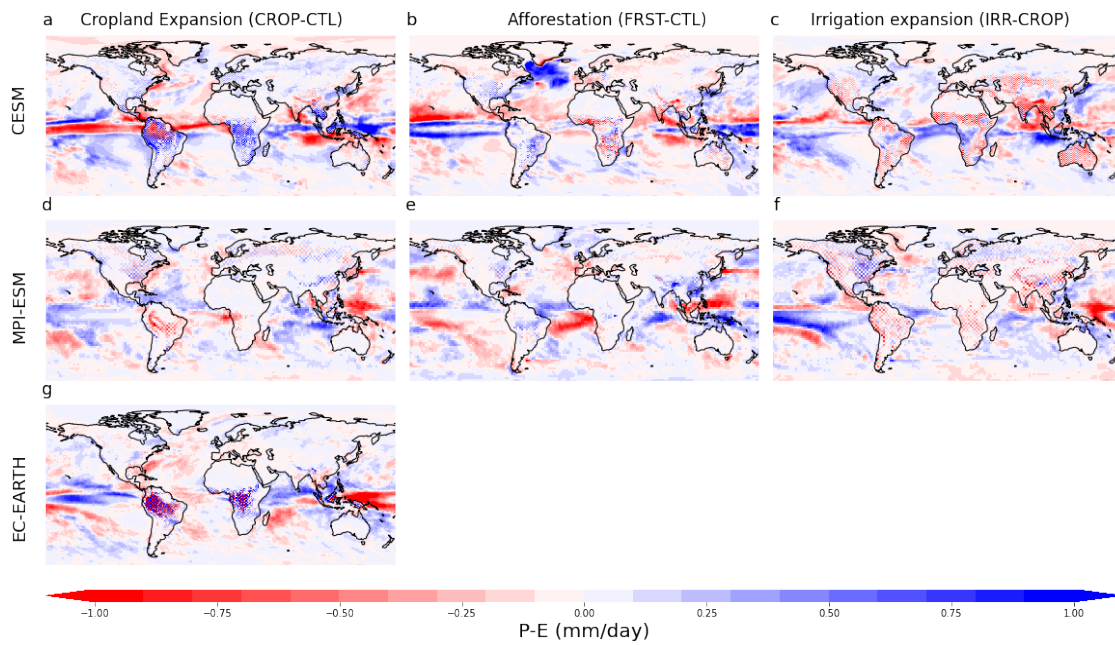
Figure C4. The seasonal mean (DJF) effects on precipitation in mm/day as a consequence of cropland expansion (CROP-CTL) in CESM (a), MPI-ESM (d) and EC-EARTH (g), for afforestation (FRST-CTL) in CESM (b) and MPI-ESM (e) and irrigation expansion (IRR-CROP) for CESM (c) and MPI-ESM (f).

Appendix D: Moisture Flux Convergence and P-E
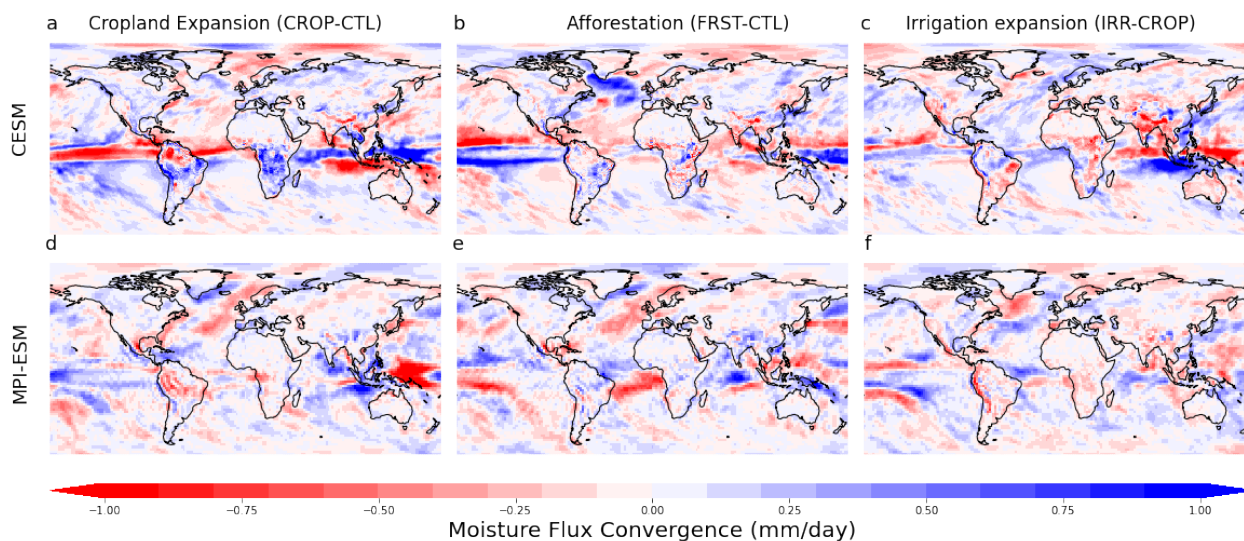
Figure D1. The mean annual impacts of land cover and land management changes on Moisture Flux Convergence (MFC) in mm/day, for cropland expansion (CROP-CTL; a,d), afforestation (FRST-CTL; b,e) and irrigation expansion(IRR-CROP; c,f) for CESM and MPI-ESM respectively. For EC-EARTH the P-E plots are available in Appendix D.

Figure D2. The annual mean effects on P-E in mm/day as a consequence of cropland expansion (CROP-CTL) in CESM (a), MPI-ESM (d) and EC-EARTH (g) for afforestation (FRST-CTL) in CESM (b) and MPI-ESM (e) and irrigation expansion (IRR-CROP) for CESM (c) and MPI-ESM (f).
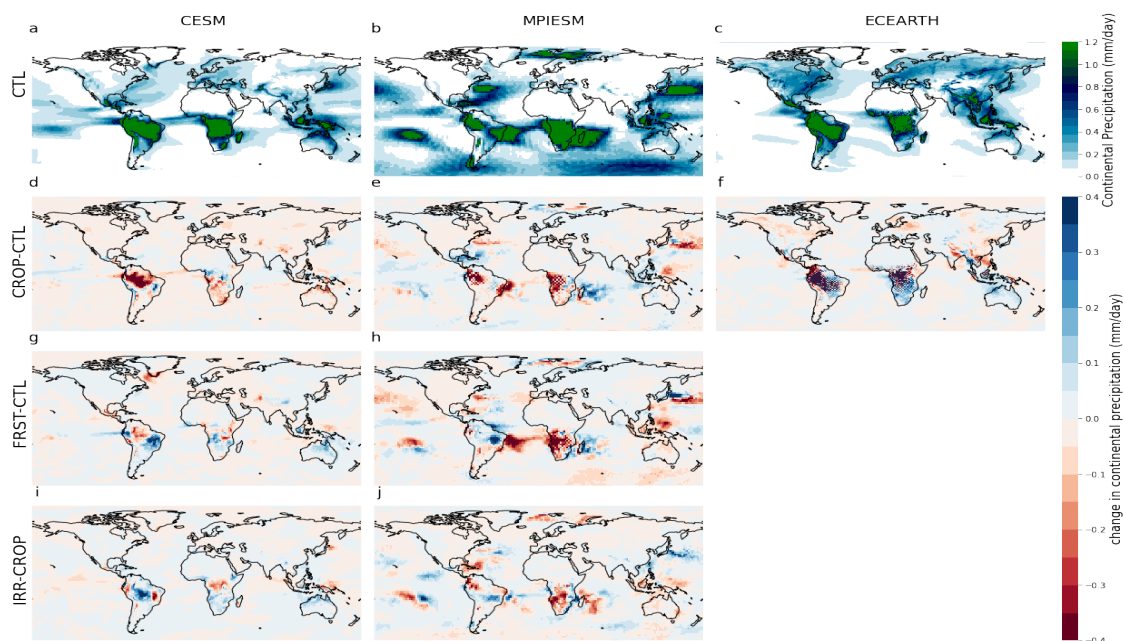
570 **Appendix E: Moisture fluxes of continental origin**

Figure E1. The annual mean continental evaporation is shown in mm/day for the CTL simulation in CESM (a), MPI-ESM (b) a,d EC-EARTH (c). The effect of cropland expansion (CROP-CTL) on the annual mean continental evaporation is shown for CESM (d), MPI-ESM (e) and EC-EARTH (f). The effect of afforestation (FRST-CTL) is shown for CESM (g) and MPI-ESM (h) and finally the effect of irrigation expansion (IRR-CROP) is shown for CESM (i) and MPI-ESM (j).
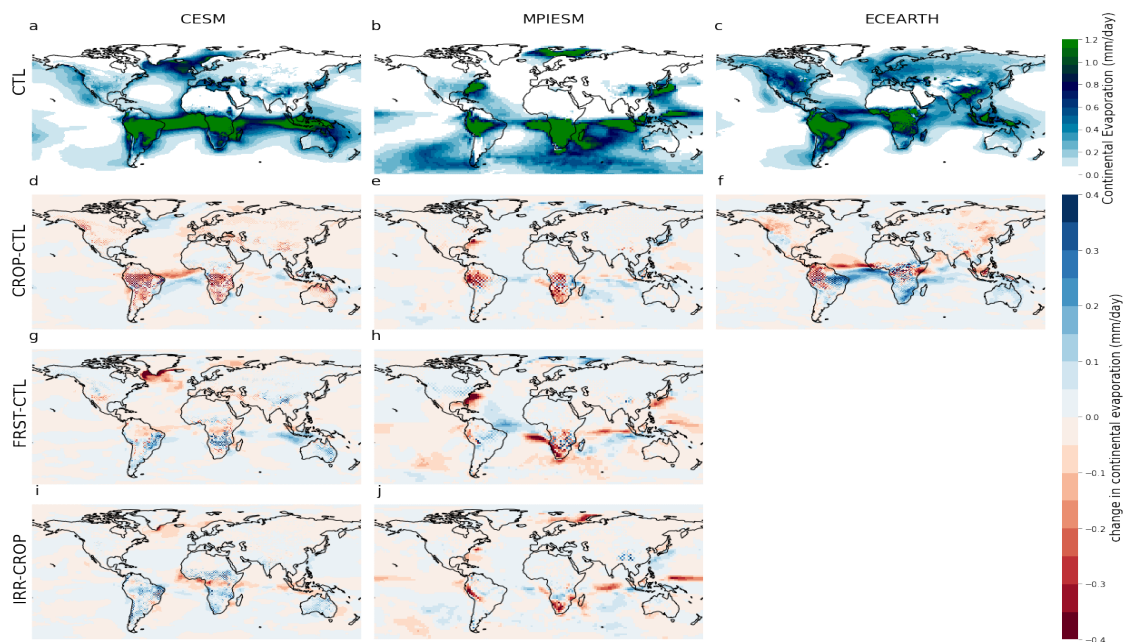
Earth System
Dynamics
Discussions

Figure E2. The annual mean continental precipitation is shown in mm/day for the CTL simulation in CESM (a), MPI-ESM (b) a,d EC-EARTH (c). The effect of cropland expansion (CROP-CTL) on the annual mean continental precipitation is shown for CESM (d), MPI-ESM (e) and EC-EARTH (f). The effect of afforestation (FRST-CTL) is shown for CESM (g) and MPI-ESM (h) and finally the effect of irrigation expansion (IRR-CROP) is shown for CESM (i) and MPI-ESM (j).

Table E1. Summary of annual total values of P, Pc, ρ_c, E, Ec, ϵ_c for the different simulations and ESMs. The absolute values are given in $km^3/year$.

CESM	P	Pc	ρ_c	E	Ec	ϵ_c
CTL	4359380	677025	0.155	2519998	659515	0.262
CROP	4244858	628946	0.148	2329935	599010	0.257
FRST	4356876	688149	0.158	2544179	671143	0.264
IRR	4300741	647669	0.151	2492105	626196	0.251
MPI-ESM	P	Pc	ρ_c	E	Ec	ϵ_c
CTL	3304814	468189	0.141	2065653	434761	0.210
CROP	3193252	438837	0.137	1942738	413053	0.213
FRST	3411430	43719	0.133	2168825	437156	0.201
IRR	3130711	431297	0.138	1988772	410919	0.207
EC-EARTH	P	Pc	ρ_c	E	Ec	ϵ_c
CTL	3597150	749179	0.208	2437720	72247	0.296
CROP	3625020	754114	0.208	2433458	720834	0.296

Author contributions. W.T., S.D.H., Q.L., J.P., F.L., S.G., I.M., F.L., C.E.L.F., J.K., D.M. and R.v.d.E. set up the idea for the analysis and helped design the study. S.D.H. and C.E.L.F. performed the analysis and adapted the WAM-2layers model to ingest the LAMACLIMA simulation data. S.D.H. performed the calculations and wrote the paper. All authors commented on the paper and provided feedback throughout the data analysis.

575 *Competing interests.* Sonia Seneviratne is member of the editorial board of the journal ESD. The authors have no other competing interests to declare.

References

Akkermans, T., Thiery, W., and Van Lipzig, N. P.: The regional climate impact of a realistic future deforestation scenario in the Congo Basin, Journal of Climate, 27, 2714–2734, 2014.

590   Banacos, P. and Schultz, D.: The Use of Moisture Flux Convergence in Forecasting Convective Initiation: Historical and Operational Perspectives, Weather and Forecasting, 20, 351–366, https://doi.org/10.1175/WAF858.1, 2005.

Baudena, M., Tuinenburg, O. A., Ferdinand, P. A., and Staal, A.: Effects of land-use change in the Amazon on precipitation are likely underestimated, Global Change Biology, 27, 5580–5587, 2021.

Benedict, I., van Heerwaarden, C., van der Ent, R., Weerts, A., and Hazeleger, W.: Decline in Terrestrial Moisture Sources of the Mississippi
595   River Basin in a Future Climate, Journal of Hydrometeorology, 21, https://doi.org/10.1175/JHM-D-19-0094.1, 2020.

Bonan, G. B.: Forests and climate change: forcings, feedbacks, and the climate benefits of forests, science, 320, 1444–1449, 2008.

Bosmans, J., van der Ent, R., Haarsma, R., Drijfhout, S., and Hilgen, F.: Precession-and obliquity-induced changes in moisture sources for enhanced precipitation over the Mediterranean Sea, Paleoceanography and Paleoclimatology, 35, e2019PA003 655, 2020.

Bowen, I. S.: The ratio of heat losses by conduction and by evaporation from any water surface, Physical review, 27, 779, 1926.

600   Boysen, L. R., Brovkin, V., Pongratz, J., Lawrence, D. M., Lawrence, P., Vuichard, N., Peylin, P., Liddicoat, S., Hajima, T., Zhang, Y., Rocher, M., Delire, C., Séférian, R., Arora, V. K., Nieradzik, L., Anthoni, P., Thiery, W., Laguë, M. M., Lawrence, D., and Lo, M. H.: Global climate response to idealized deforestation in CMIP6 models, Biogeosciences, 17, 5615–5638, https://doi.org/10.5194/bg-17-5615-2020, 2020.

Brubaker, K. L., Entekhabi, D., and Eagleson, P.: Estimation of continental precipitation recycling, Journal of Climate, 6, 1077–1089, 1993.

Cook, K.: South American Climate Variability and Change: Remote and Regional Forcing Processes, pp. 193–212,
605   https://doi.org/10.1007/978-90-481-2672-9_8, 2009.

Corless, R. M., Gonnet, G. H., Hare, D. E., Jeffrey, D. J., and Knuth, D. E.: On the LambertW function, Advances in Computational mathematics, 5, 329–359, 1996.

De Hertog, S. J., Havermann, F., Vanderkelen, I., Guo, S., Luo, F., Manola, I., Coumou, D., Davin, E. L., Duveiller, G., Lejeune, Q., Pongratz, J., Schleussner, C. F., Seneviratne, S. I., and Thiery, W.: Earth System Dynamics, 14, 629–667, https://doi.org/10.5194/egusphere-2023-
610   253, 2023.

de Vrese, P., Hagemann, S., and Claussen, M.: Asian irrigation, African rain: Remote impacts of irrigation, Geophysical Research Letters, 43, 3737–3745, https://doi.org/10.1002/2016GL068146, 2016.

Deser, C., Knutti, R., Solomon, S., and Phillips, A. S.: Communication of the role of natural variability in future North American climate, Nature Climate Change, 2, 775–779, 2012.

615   Deser, C., Lehner, F., Rodgers, K. B., Ault, T., Delworth, T. L., DiNezio, P. N., Fiore, A., Frankignoul, C., Fyfe, J. C., Horton, D. E., et al.: Insights from Earth system model initial-condition large ensembles and future prospects, Nature Climate Change, 10, 277–286, 2020.

Devaraju, N., de Noblet-Ducoudré, N., Quesada, B., and Bala, G.: Quantifying the relative importance of direct and indirect biophysical effects of deforestation on surface temperature and teleconnections, Journal of Climate, 31, 3811–3829, https://doi.org/10.1175/JCLI-D-17-0563.1, 2018.

620   Dominguez, F., Kumar, P., Liang, X.-Z., and Ting, M.: Impact of atmospheric moisture storage on precipitation recycling, Journal of climate, 19, 1513–1530, 2006.

Findell, K. L., Keys, P. W., van der Ent, R. J., Lintner, B. R., Berg, A., and Krasting, J. P.: Rising temperatures increase importance of oceanic evaporation as a source for continental precipitation, Journal of Climate, 32, 7713–7726, 2019.

Earth System
Dynamics
Discussions

Open Access

EGU

Gimeno, L., Stohl, A., Trigo, R. M., Dominguez, F., Yoshimura, K., Yu, L., Drumond, A., Durán-Quesada, A. M., and Nieto, R.: Oceanic
625 and terrestrial sources of continental precipitation, Reviews of Geophysics, 50, 2012.

Gimeno, L., Vázquez, M., Eiras-Barca, J., Sorí, R., Stojanovic, M., Algarra, I., Nieto, R., Ramos, A. M., Durán-Quesada, A. M., and
Dominguez, F.: Recent progress on the sources of continental precipitation as revealed by moisture transport analysis, Earth-Science
Reviews, 201, 103 070, 2020.

Goessling, H. and Reick, C.: What do moisture recycling estimates tell us? Exploring the extreme case of non-evaporating continents,
630 Hydrology and Earth System Sciences, 15, 3217–3235, 2011.

Guimberteau, M., Laval, K., Perrier, A., and Polcher, J.: Global effect of irrigation and its impact on the onset of the Indian summer monsoon,
Climate Dynamics, 39, 1329–1348, 2012.

Guo, L., Van Der Ent, R. J., Klingaman, N. P., Demory, M.-E., Vidale, P. L., Turner, A. G., Stephan, C. C., and Chevuturi, A.: Effects of
horizontal resolution and air–sea coupling on simulated moisture source for East Asian precipitation in MetUM GA6/GC2, Geoscientific
635 Model Development, 13, 6011–6028, 2020.

Hauser, M., Thiery, W., and Seneviratne, S. I.: Potential of global land water recycling to mitigate local temperature extremes, Earth System
Dynamics, 10, 157–169, 2019.

Hoek van Dijke, A. J., Herold, M., Mallick, K., Benedict, I., Machwitz, M., Schlerf, M., Pranindita, A., Theeuwen, J. J., Bastin, J.-F., and
Teuling, A. J.: Shifts in regional water availability due to global tree restoration, Nature Geoscience, 15, 363–368, 2022.

640 Laguë, M. M., Bonan, G. B., and Swann, A. L.: Separating the impact of individual land surface properties on the terrestrial surface energy
budget in both the coupled and uncoupled land–atmosphere system, Journal of Climate, 32, 5725–5744, https://doi.org/10.1175/JCLI-D-
18-0812.1, 2019.

Lawrence, D. M., Hurtt, G. C., Arneth, A., Brovkin, V., Calvin, K. V., Jones, A. D., Jones, C. D., Lawrence, P. J., de Noblet-Ducoudré, N.,
Pongratz, J., et al.: The Land Use Model Intercomparison Project (LUMIP) contribution to CMIP6: rationale and experimental design,
645 Geoscientific Model Development, 9, 2973–2998, 2016.

Li, Z., Liu, T., Huang, Y., Peng, J., and Ling, Y.: Evaluation of the CMIP6 precipitation simulations over global land, Earth's Future, 10,
e2021EF002 500, 2022.

Lombardozzi, D. L., Lu, Y., Lawrence, P. J., Lawrence, D. M., Swenson, S., Oleson, K. W., Wieder, W. R., and Ainsworth, E. A.: Simulating
agriculture in the Community Land Model version 5, Journal of Geophysical Research: Biogeosciences, 125, e2019JG005 529, 2020.

650 Luyssaert, S., Jammet, M., Stoy, P. C., Estel, S., Pongratz, J., Ceschia, E., Churkina, G., Don, A., Erb, K., Ferlicoq, M., et al.: Land manage-
ment and land-cover change have impacts of similar magnitude on surface temperature, Nature Climate Change, 4, 389–393, 2014.

Mahmood, R., Pielke Sr, R. A., Hubbard, K. G., Niyogi, D., Dirmeyer, P. A., McAlpine, C., Carleton, A. M., Hale, R., Gameda, S., Beltrán-
Przekurat, A., et al.: Land cover changes and their biogeophysical effects on climate, International journal of climatology, 34, 929–953,
2014.

655 Mbow, H.-O. P., Reisinger, A., Canadell, J., and O'Brien, P.: Special Report on climate change, desertification, land degradation, sustainable
land management, food security, and greenhouse gas fluxes in terrestrial ecosystems (SR2), Ginevra, IPCC, 2017.

Pongratz, J., Reick, C., Raddatz, T., and Claussen, M.: Biogeophysical versus biogeochemical climate response to historical anthropogenic
land cover change, Geophysical Research Letters, 37, 2010.

Pongratz, J., Schwingshackl, C., Bultan, S., Obermeier, W., Havermann, F., and Guo, S.: Land use effects on climate: current state, recent
660 progress, and emerging topics, Current Climate Change Reports, pp. 1–22, 2021.

Earth System
Dynamics
Discussions

Portmann, R., Beyerle, U., Davin, E., Fischer, E. M., De Hertog, S., and Schemm, S.: Global forestation and deforestation affect remote climate via adjusted atmosphere and ocean circulation, Nature Communications, 13, 1–11, 2022.

Puma, M. and Cook, B.: Effects of irrigation on global climate during the 20th century, Journal of Geophysical Research: Atmospheres, 115, 2010.

665 Rogelj, J., Shindell, D., Jiang, K., Fifita, S., Forster, P., Ginzburg, V., Handa, C., Kheshgi, H., Kobayashi, S., Kriegler, E., et al.: Mitigation pathways compatible with 1.5 C in the context of sustainable development, pp. 93–174, 2018.

Seneviratne, S. I., Wartenburger, R., Guillod, B. P., Hirsch, A. L., Vogel, M. M., Brovkin, V., van Vuuren, D. P., Schaller, N., Boysen, L., Calvin, K. V., et al.: Climate extremes, land–climate feedbacks and land-use forcing at 1.5 C, Philosophical Transactions of the Royal Society A: Mathematical, Physical and Engineering Sciences, 376, 20160450, 2018.

670 Shukla, J. and Mintz, Y.: Influence of land-surface evapotranspiration on the Earth's climate, Science, 215, 1498–1501, 1982.

Spracklen, D., Baker, J., Garcia-Carreras, L., and Marsham, J.: The effects of tropical vegetation on rainfall, Annual Review of Environment and Resources, 2018.

Spracklen, D. V., Arnold, S. R., and Taylor, C.: Observations of increased tropical rainfall preceded by air passage over forests, Nature, 489, 282–285, 2012.

675 Staal, A., Tuinenburg, O. A., Bosmans, J. H., Holmgren, M., van Nes, E. H., Scheffer, M., Zemp, D. C., and Dekker, S. C.: Forest-rainfall cascades buffer against drought across the Amazon, Nature Climate Change, 8, 539–543, 2018.

Theeuwen, J. J., Staal, A., Tuinenburg, O. A., Hamelers, B. V., and Dekker, S. C.: Local moisture recycling across the globe, Hydrology and Earth System Sciences, 27, 1457–1476, 2023.

Thiery, W., Davin, E. L., Seneviratne, S. I., Bedka, K., Lhermitte, S., and van Lipzig, N. P.: Hazardous thunderstorm intensification over 680 Lake Victoria, Nature communications, 7, 1–7, 2016.

Thiery, W., Davin, E. L., Lawrence, D. M., Hirsch, A. L., Hauser, M., and Seneviratne, S. I.: Present-day irrigation mitigates heat extremes, Journal of Geophysical Research, 122, 1403–1422, https://doi.org/10.1002/2016JD025740, 2017.

Thiery, W., Visser, A. J., Fischer, E. M., Hauser, M., Hirsch, A. L., Lawrence, D. M., Lejeune, Q., Davin, E. L., and Seneviratne, S. I.: Warming of hot extremes alleviated by expanding irrigation, Nature communications, 11, 1–7, 2020.

685 Tuinenburg, O., Hutjes, R., Stacke, T., Wiltshire, A., and Lucas-Picher, P.: Effects of irrigation in India on the atmospheric water budget, Journal of Hydrometeorology, 15, 1028–1050, 2014.

Tuinenburg, O. A., Theeuwen, J. J., and Staal, A.: High-resolution global atmospheric moisture connections from evaporation to precipitation, Earth System Science Data, 12, 3177–3188, 2020.

Van de Walle, J., Thiery, W., Brousse, O., Souverijns, N., Demuzere, M., and Lipzig, N.: A convection-permitting model for the Lake 690 Victoria Basin: evaluation and insight into the mesoscale versus synoptic atmospheric dynamics, Climate Dynamics, 54, 1779–1799, https://doi.org/10.1007/s00382-019-05088-2, 2020.

van der Ent, R. and Savenije, H.: Length and time scales of atmospheric moisture recycling, Atmospheric Chemistry and Physics, 11, 1853–1863, 2011.

van der Ent, R., Wang-Erlandsson, L., Keys, P. W., and Savenije, H.: Contrasting roles of interception and transpiration in the hydrological 695 cycle–Part 2: Moisture recycling, Earth System Dynamics, 5, 471–489, 2014.

van der Ent, R. J., Savenije, H. H., Schaefli, B., and Steele-Dunne, S. C.: Origin and fate of atmospheric moisture over continents, Water Resources Research, 46, 1–12, https://doi.org/10.1029/2010WR009127, 2010.

Earth System
Dynamics
Discussions

Wang, J., Chagnon, F., Williams, E., Betts, A., Rennó, N., Machado, L., Bisht, G., Knox, R., and Bras, R.: Impact of deforestation in the Amazon Basin on cloud climatology, Proceedings of the National Academy of Sciences of the United States of America, 106, 3670–4, https://doi.org/10.1073/pnas.0810156106, 2009.

700 Wang-Erlandsson, L., Fetzer, I., Keys, P., Ent, R., Savenije, H., and Gordon, L.: Remote land use impacts on river flows through atmospheric teleconnections, Hydrology and Earth System Sciences, 22, 4311–4328, https://doi.org/10.5194/hess-22-4311-2018, 2018.

Winckler, J., Reick, C. H., and Pongratz, J.: Robust identification of local biogeophysical effects of land-cover change in a global climate model, Journal of Climate, 30, 1159–1176, 2017a.

705 Winckler, J., Reick, C. H., and Pongratz, J.: Why does the locally induced temperature response to land cover change differ across scenarios?, Geophysical Research Letters, 44, 3833–3840, 2017b.

Winckler, J., Lejeune, Q., Reick, C. H., and Pongratz, J.: Nonlocal effects dominate the global mean surface temperature response to the biogeophysical effects of deforestation, Geophysical Research Letters, 46, 745–755, 2019.

Wunderling, N., Staal, A., Sakschewski, B., Hirota, M., Tuinenburg, O. A., Donges, J. F., Barbosa, H. M., and Winkelmann, R.: Recurrent
710 droughts increase risk of cascading tipping events by outpacing adaptive capacities in the Amazon rainforest, Proceedings of the National Academy of Sciences, 119, e2120777119, 2022.